Check for updates

Received: 13 July 2024 | Accepted: 2 October 2024

DOI: 10.1111/mice.13357

COMPUTER-AIDED CIVIL AND INFRASTRUCTURE ENGINEERING WILEY

RESEARCH ARTICLE

Natural language processing-based deep transfer learning model across diverse tabular datasets for bond strength prediction of composite bars in concrete

Pei-Fu Zhang[1] | **Daxu Zhang**[1] | **Xiao-Ling Zhao**[2] | **Xuan Zhao**[1] | **Mudassir Iqbal**[1,3] | **Yiliyaer Tuerxunmaimaiti**[1] | **Qi Zhao**[2]

[1]State Key Laboratory of Ocean Engineering, Shanghai Key Laboratory for Digital Maintenance of Buildings and Infrastructure, School of Ocean and Civil Engineering, Shanghai Jiao Tong University, Shanghai, China

[2]Department of Civil and Environmental Engineering, The Hong Kong Polytechnic University, Hong Kong, China

[3]Department of Civil Engineering, University of Engineering and Technology, Peshawar, Pakistan

Correspondence
Daxu Zhang, Department of Civil Engineering, Shanghai Jiao Tong University, 800 Dongchuan Road, Shanghai, China.
Email: daxu.zhang@sjtu.edu.cn

Xiao-Ling Zhao, Department of Civil and Environmental Engineering, The Hong Kong Polytechnic University, Hong Kong, China.
Email: xiao-lin.zhao@polyu.edu.hk

Funding information
National Natural Science Foundation of China, Grant/Award Numbers: 12072192, U1831105; Shanghai Municipal Natural Science Foundation, Grant/Award Number: 20ZR1429500

Abstract

As conventional machine learning models often struggle with scarcity and structural variation of training data, this paper proposes a novel regression transfer learning framework called transferable tabular regressor (TransTabRegressor) to address this challenge. The TransTabRegressor integrates natural language processing (NLP) for feature encoding, transformer for enhanced feature representation, and deep learning (DL) for robust modeling, facilitating effective transfer learning across tabular datasets using reducing input parameters. By leveraging the NLP data processor, the framework embeds both parameter names and values, enabling it to recognize and adapt to different expressions of similar parameters. For instance, the bond strength of fiber-reinforced polymer (FRP) bars embedded in ultra-high-performance concrete (UHPC) is critical for ensuring the integrity of FRP-UHPC structures. While pullout tests are widely adopted for their simplicity to generate substantial data, beam tests provide a closer approximation to actual stress conditions but are more complex thus resulting in limited data size. As a verification, the framework is applied to predict the bond strength of FRP bars embedded in UHPC using limited beam test data. A pre-trained model is first established using 479 pieces of pullout test data. Subsequently, two transfer learning models are developed by fine-tuning on 115 pieces of beam test data, where 66 correspond to concrete splitting failure and 49 correspond to pullout failure. For comparative analysis, XGBoost and neural network models are directly trained on the beam test data. Evaluation results demonstrate that the transfer learning models achieve significantly improved prediction accuracy and generalization capability. This study significantly highlights the effectiveness of the proposed TransTabRegressor in handling data scarcity and variability in input parameters across various engineering applications.

This is an open access article under the terms of the Creative Commons Attribution-NonCommercial-NoDerivs License, which permits use and distribution in any medium, provided the original work is properly cited, the use is non-commercial and no modifications or adaptations are made.
© 2024 The Author(s). *Computer-Aided Civil and Infrastructure Engineering* published by Wiley Periodicals LLC on behalf of Editor.

1 | INTRODUCTION

Ultra-high-performance concrete (UHPC) and fiber-reinforced polymer (FRP) bars have emerged as highly advantageous materials in modern construction due to their exceptional mechanical properties and durability (Du et al., 2021; Zhao, Zhao, Zhang, Dai, & Xue., 2024). UHPC offers superior compressive strength, durability, and resistance to environmental degradation (B. T. Huang et al., 2021; Saleh et al., 2023; Teng et al., 2019), while FRP bars provide high tensile strength, corrosion resistance, and lightweight characteristics (Zhao et al., 2021; Zhao, Zhao, Zhang, & Duan, 2024). The effective integration of these two materials can significantly enhance structural performance in particular applications, such as bridges and marine structures (Zeng et al., 2022a). However, the relatively low deformation modulus of FRP bars may make it difficult for these materials to resist shear cracks, which typically leads to sudden brittle failure and results in an economically inefficient extension of the reinforcement area (Gribniak et al., 2013). Furthermore, creep rupture reduces the long-term strength of FRP materials (Rossini et al., 2019). Therefore, a crucial aspect of ensuring the structural integrity of FRP-UHPC composites is the bond strength between FRP bars and UHPC (Hung et al., 2021), which directly affects load transfer and the overall performance of the structure.

Extensive experimental research has been conducted to investigate the bond strength of glass FRP (GFRP) bars embedded in UHPC, where two primary testing methods are utilized regarding pullout tests (Hossain et al., 2018; Hu et al., 2023; Kim & Wang, 2022; Liang et al., 2023; R. Pan et al., 2022, 2023; R. S. Pan et al., 2023; Sayed-Ahmed & Sennah, 2015, 2016; Tong et al., 2023; D. Y. Yoo & Yoon, 2017; D. Y. Yoo et al., 2015; S. J. Yoo et al., 2023; Zeng et al., 2022b) and beam tests (Hossain et al., 2017; Hu et al., 2024; Kauffman & Fam, 2024; Michaud et al., 2021). Pullout tests are favored for their simplicity in setup and execution, leading to a large volume of available data (ACI Committee 408, 2003). In contrast, beam tests are more complex and time-consuming, resulting in fewer studies and less data (S. J. Yoo et al., 2024). However, pullout tests primarily subject the FRP bars to tensile forces and the concrete to compressive forces, whereas beam tests involve both the FRP bars and the concrete in tensile stress (ACI Committee 408, 2003). This makes beam tests more representative of the actual stress conditions in real structural applications, providing a more accurate reflection of the bond performance between FRP and UHPC (Hu et al., 2024). Additionally, it is important to note that the beam test was originally designed for steel bars. The friction generated between FRP bars and concrete near the hinged gap artificially increases bonding stresses (Gudonis et al., 2014), indicating that further research is needed to adapt this method effectively for FRP bars.

Machine learning (ML) has shown great promise in engineering areas (Naser, 2021; Thai, 2022) due to its ability to handle large datasets and uncover complex relationships within the experimental data (Jiang & Adeli, 2005; Rafiei & Adeli, 2018). Extensive research has been conducted using ML for predicting material properties (Rafiei et al., 2016), optimizing material design (Rafiei et al., 2017), and forecasting structural performance (Bakouregui et al., 2021; Das et al., 2019; Shafigh, 2024). Previous studies have successfully applied ML techniques (Hernandez Obando et al., 2024; Iqbal, Zhang, Khan, et al., 2023; Iqbal, Zhang, Khan, et al., 2023), such as effective extreme gradient boosting (XGBoost) and neural networks (NNs), to predict the bond strength of FRP in various types of concrete (Basaran et al., 2021; Yan et al., 2017), including ordinary concrete (Jahangir & Rezazadeh Eidgahee, 2021; Kumar et al., 2024; F. Zhang et al., 2023), seawater sea sand concrete (P.-F. Zhang, Iqbal, et al., 2024), and UHPC (P.-F. Zhang, Zhao, et al., 2024). These studies highlight the maturity and potential of ML methods in this field. However, the beam test data for FRP-UHPC bond strength is limited to approximately 100 data points, where around 60 representing concrete splitting failure and 40 for pullout failure, whereas the pullout test data includes over 400 data points. Pullout failure generally involves the gradual extraction of the FRP bar from the concrete with minimal cracking, whereas splitting failure occurs due to insufficient tensile resistance of the concrete, leading to longitudinal cracks along the direction of the FRP bar (S. J. Yoo et al., 2024). Given these significant differences, it is crucial to model these two failure modes separately when applying machine learning. The scarcity of FRP-UHPC beam test data poses a significant challenge for the direct application of ML, as the limited data might lead to poor model performance and generalization.

To overcome the limitations posed by the small amount of beam test data, transfer learning offers a viable solution (S. J. Pan & Yang, 2010; Radford et al., 2021; Shin et al., 2016). Transfer learning is an ML technique that improves the performance of a model in a target domain by leveraging knowledge from a related source domain with abundant data (Luo & Paal, 2021; Nan et al., 2024; Z. Zhang et al., 2022). This approach has been successfully applied in various fields, including engineering, where it reduces the need for large datasets in the target domain by transferring insights from a related domain with abundant data (Jung et al., 2022; Pak et al., 2023; Xu et al., 2021). Deep learning, a subset of ML that utilizes NNs with multiple layers to automatically learn representations from large datasets (Alam et al., 2020; Martins et al., 2020), has further advanced the ability to model complex relationships and extract intricate

14678667, 2025, 7, Downloaded from https://onlinelibrary.wiley.com/doi/10.1111/mice.13357 by HONG KONG POLYTECHNIC UNIVERSITY HU NG HOM, Wiley Online Library on [11/03/2025]. See the Terms and Conditions (https://onlinelibrary.wiley.com/terms-and-conditions) on Wiley Online Library for rules of use; OA articles are governed by the applicable Creative Commons License

features from data (Rafiei & Adeli, 2017; Rafiei et al., 2024). Additionally, integrating deep learning techniques with transfer learning has emerged as a promising direction (S. Z. Chen & Feng, 2022; Nogay & Adeli, 2021; Zou & Chung, 2024), allowing for more sophisticated feature extraction and improved generalization across different datasets. However, traditional transfer learning methods, often require consistent data structures between the source and target domains (Cholakov & Kolev, 2022; X. Huang et al., 2020). Given the differences in test conditions and data availability, the input parameters for ML models of pullout and beam tests are not always consistent.

To address the challenge of transferring knowledge across tables with disparate input parameters, a versatile tabular learning framework has been proposed for classification tasks involving tabular data (Wang & Sun, 2022). This approach transforms the basic elements of tabular data modeling from columns in traditional ML to tokens in natural language processing (NLP; Devlin et al., 2019; Raffel et al., 2020). By contextualizing both names and values of parameters, the model can generalize across different tables. Using tokenization and embedding techniques in NLP, transformers (X. Huang et al., 2020; Vaswani et al., 2017) capture complex dependencies and relationships within the data, making them highly effective for subsequent deep learning tasks. Deep learning techniques are then used to train the processed data. Through NLP processing of tabular data and enhanced representation by transformers, the deep learning model can be pre-trained and then fine-tuned to achieve the transfer learning task. This approach has been successfully applied to transfer learning for classification tasks, highlighting its potential for regression prediction tasks.

Despite the significant advancements in ML for bond strength prediction, a notable research gap persists in the accurate prediction of bond strength for FRP bars in UHPC using beam test data. While beam tests provide a more realistic representation of the actual stress conditions in structures, compared to the pullout test, their complexity and the resulting scarcity of data pose a substantial challenge. Although there are over 400 pieces of pullout test data, the available beam test data for FRP-UHPC bond strength are limited to approximately 60 points for concrete splitting failure and 40 points for pullout failure. Traditional ML models struggle with this limited beam test data, leading to poor model performance and generalization. Transfer learning emerges as a promising solution to this problem by leveraging knowledge from domains with abundant data (pullout test) to improve prediction accuracy in domains with limited data (beam test). However, traditional transfer learning methods often require consistent data structures between the source and target domains, which is not feasible given the differences in test conditions and available data for pullout and beam tests. The input parameters for pullout and beam tests are not always consistent, further complicating the direct application of traditional transfer learning methods.

To address this research gap, this study proposes a transferable tabular regressor (TransTabRegressor) framework that leverages NLP, transformers, and DL techniques to transfer knowledge of bond strength from pullout test data to beam test data. The novelty of this approach lies in its ability to handle different input parameters and leverage limited beam test data through advanced NLP and DL techniques. Significantly, the NLP technique processes both the values and names of input parameters, enabling deep learning models to accept data with varying parameters. This framework establishes a solid foundation for transferring information from a pre-trained model, built on extensive data with more input parameters, to a transfer learning model, which operates with a smaller dataset and fewer input parameters. Specifically, the framework begins with establishing a pre-trained model based on 479 pullout test data points considering concrete splitting failure and pullout failure. The transfer learning models are then developed by fine-tuning the pre-trained model using 66 beam test data points in case of concrete splitting failure and 49 data points of pullout failure. For comparison, XGBoost and NN models are directly trained on the 66 and 79 pieces of beam test data. The established models are subsequently evaluated using regression criteria. In summary, the proposed TransTabRegressor framework involves fine-tuning a pre-trained model on an extensive pullout test dataset to improve predictions for limited beam test data, demonstrating the potential of advanced NLP and DL-based transfer learning methods in structural engineering applications.

The remainder of this paper is organized as follows. Section 2 describes the principles of the proposed transfer learning framework TransTabRegressor. The framework combines an NLP data processor, transformer, deep learning network, and transfer learning model. Sections 3 and 4 introduce the dataset and development of transfer learning models. Section 5 presents the evaluation and transferable ability of transfer learning models, as well as the extensible modelling capacity of the proposed framework. Section 6 presents the conclusions of this work.

2 | METHODOLOGY

2.1 | TransTabRegressor

Existing ML models for tabular data typically require the same table structure for both training and testing, which makes it challenging to learn across tables with different structures. To address this issue, Wang and Sun (2022) proposed the Transferable Tabular Transformer

14678667, 2025, 7, Downloaded from https://onlinelibrary.wiley.com/doi/10.1111/mice.13357 by HONG KONG POLYTECHNIC UNIVERSITY HU NG HOM, Wiley Online Library on [11/03/2025]. See the Terms and Conditions (https://onlinelibrary.wiley.com/terms-and-conditions) on Wiley Online Library for rules of use; OA articles are governed by the applicable Creative Commons License

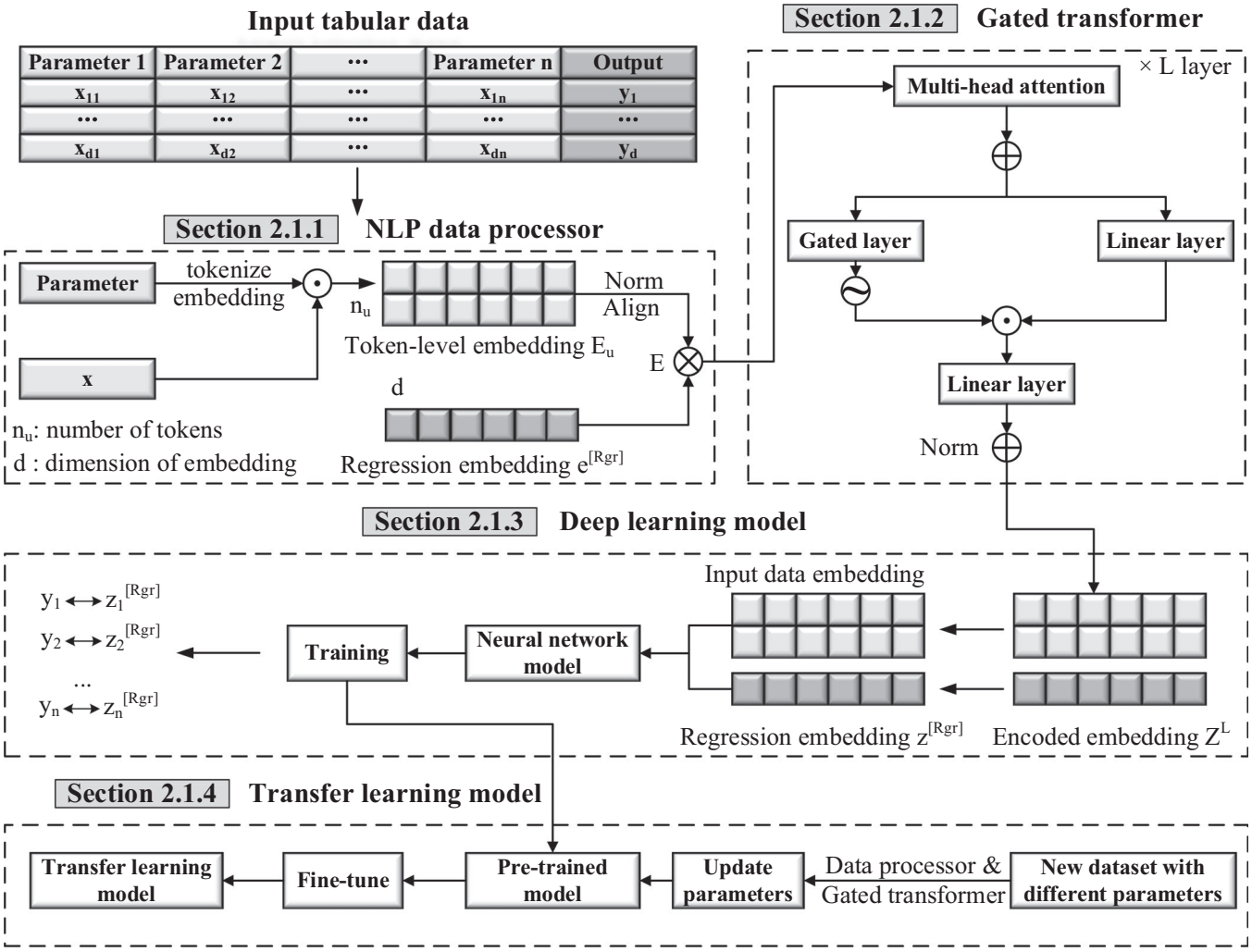

FIGURE 1 Note The demonstration of TransTabRegressor framework. (Note: ⊙ is element-wise multiply, ⊕ is element-wise add, ⊗ is concatenate, and ⊖ is positional encoding).

(TransTab). The TransTab algorithm integrates DL and NLP techniques (Cholakov & Kolev, 2022; X. Huang et al., 2020) to transfer knowledge across tables with disparate columns by encoding parameter names and values into token-level embeddings, which are fundamental elements in NLP (Devlin et al., 2019). This process allows the model to consider both the names and values of parameters during modeling. The TransTab framework consists of three primary components: (1) the input NLP processor, which tokenizes the input tabular data and embeds them into embeddings; (2) the gated transformer that further processes the token-level embeddings; and (3) the classifier learning module, which is trained for classification tasks.

Motivated by the TransTab, this paper proposes a TransTabRegressor framework for regression and transfer learning of numerical tabular data. The framework combines an NLP data processor, a gated transformer, a regression deep learning model, and a transfer learning model. Figure 1 illustrates the workflow of TransTabRegressor. The NLP data processor converts the data into token-level embeddings $\mathbf{E}$, which are then further encoded by the L-layer gated transformer into $\mathbf{Z}^L$. The regression embeddings $\mathbf{z}^{[Rgr]}$ after gated transformer are leveraged to the deep learning models to make regression predictions. Subsequently, the transfer learning models are developed by adjusting the dimensions of input parameters and fine-tuning pre-trained models.

2.1.1 | NLP data processor

The NLP data processor (Wang & Sun, 2022) converts tabular data (both names and values of parameters) into a sequence of semantically encoded token-level embeddings. This means both names and values of input parameters are encoded to the basic elements, incorporating the semantic information of names and the numerical knowledge of values into prediction modelling. Thus, this

14678667, 2025, 7, Downloaded from https://onlinelibrary.wiley.com/doi/10.1111/mice.13357 by HONG KONG POLYTECHNIC UNIVERSITY HU NG HOM, Wiley Online Library on [11/03/2025]. See the Terms and Conditions (https://onlinelibrary.wiley.com/terms-and-conditions) on Wiley Online Library for rules of use; OA articles are governed by the applicable Creative Commons License

allows the models to retain and transfer the knowledge across tabular datasets with diverse parameters.

For the numerical parameters, the parameter names and values are not directly concatenated because the tokenization-embedding approach tends to perform poorly in differentiating numbers (Lin et al., 2020). In detail, the parameter names are firstly tokenized and matched to the Bert token embedding matrix (Devlin et al., 2019). The parameter name embedding $\mathbf{E}_{u,par} \in \mathbb{R}^{n_u \times d}$ is generated, where n_u is the number of tokens and d is the embedding dimension. Then the numerical values are element-wise multiplied by the parameter embedding (Wang & Sun, 2022), to yield the numerical embedding as $\mathbf{E}_u = x_u \odot \mathbf{E}_{u,par}$, where x_u represents the standardized numerical values, and $\mathbf{E}_{u,par}$ is the parameter embedding for numerical features. This element-wise multiplication means that each numerical value is multiplied by its corresponding element in the parameter embedding, integrating the numerical values with their contextual column embeddings and capturing their influence relative to the column. Finally, $\mathbf{E}_u$ undergoes layer normalization (Ba et al., 2016) and is then combined with the regression embedding $\mathbf{e}^{[Rgr]}$, obtaining the overall embedding $\mathbf{E} = \tilde{\mathbf{E}}_u \otimes \mathbf{e}^{[Rgr]}$. This approach contextualizes parameter values with corresponding parameter names, allowing for the transfer of information across tables and recognizing different but similar representations of identical parameters as equivalent.

2.1.2 | Gated transformer

The token-level embeddings are further encoded by the tabular gated transformer (Cholakov & Kolev, 2022; Wang & Sun, 2022), which is an adaption of the classical transformer in NLP areas (Vaswani et al., 2017). The gated mechanism dynamically adjusts the importance of each token embedding, better capturing the interaction and importance between parameters in tabular data, thus enhancing the model's ability to handle tabular data. The gated transformer is composed of multi-head self-attention mechanisms and gated feedforward units. It integrates a token-wise gating mechanism, improving its ability to capture intricate dependencies within tabular datasets. The multi-head-self-attention layer is used to explore the interaction relationships between parameters and obtain the final output. The multi-head-self-attention output is further fed into a token-based gating layer to control the importance of each token embedding. Then, the multi-head self-attention output undergoes gating via a gated feedforward layer. Specifically, the embedding of each token is controlled by gate values to adjust their importance. The output after gating is further input into the linear layer for transformation, and residual connections are added with the original attention output to obtain the output of the transformer model.

In detail, multi-head attention allows the model to jointly attend to information from different representation subspaces at different positions, as shown in Equations (1) and (2). The input representation $\mathbf{Z}^l$ at the lth layer is first adopted to explore the interactions between parameters.

$$\begin{aligned}\mathbf{Z}^l_{att} &= \text{MultiHeadAttn}\left(\mathbf{Z}^l\right) \\ &= [\text{head}_1, \text{head}_2, \ldots, \text{head}_h] \cdot \mathbf{W}^O \end{aligned} \tag{1}$$

$$\text{head}_i = \text{Attention}\left(\mathbf{Z}^l \cdot \mathbf{W}^Q_i, \mathbf{Z}^l \cdot \mathbf{W}^K_i, \mathbf{Z}^l \cdot \mathbf{W}^V_i\right) \tag{2}$$

where $\mathbf{Z}_0 = \mathbf{E}$ denotes the input at the first layer; $\mathbf{W}^O \in \mathbb{R}^{d \times d}$; $\mathbf{W}^Q_i, \mathbf{W}^K_i$, and $\mathbf{W}^V_i$ are weight matrices (in $\mathbb{R}^{d \times \frac{d}{h}}$) of query, key, and value of the ith head self-attention module, respectively.

The multi-head attention output $\mathbf{Z}^l_{att}$ undergoes further transformation by a token-wise gating layer as presented in Equation (3). The gating mechanism effectively filters the output of the linear layer to obtain the transformer output $\mathbf{Z}^{l+1} \in \mathbb{R}^{n \times d}$ as presented in Equation (4).

$$\mathrm{g}^l = \sigma(\mathbf{Z}^l_{att} \cdot \mathbf{w}^G) \tag{3}$$

where $\sigma(\cdot)$ denotes the sigmoid function; $\mathrm{g}^l \in [0,1]^n$ regulates the intensity of individual token embedding before $\mathbf{Z}_{att}$ proceeds to linear projection.

$$\mathbf{Z}^{l+1} = \text{Linear}\left(\left(\mathrm{g}^l \odot \mathbf{Z}^l_{att}\right) \oplus \text{Linear}\left(\mathbf{Z}^l_{att}\right)\right) \tag{4}$$

The resulting transformer output reflects the ability to focus on critical parameters by redistributing attention across tokens. Ultimately, the regression embedding $\mathbf{z}^{[Rgr]}$ at the Lth layer serves as a pivotal component for downstream regression tasks. The gated transformer offers enhanced adaptability and efficacy in capturing complex dependencies within tabular data, making it well-suited for a wide range of structured data applications.

2.1.3 | DL regression model

The encoded embeddings are fed into the NN regression module to establish a deep learning regression model. This module consists of one or more hidden layers, which can be configured based on the complexity of the dataset. Each hidden layer utilizes the rectified linear unit (ReLU) activation function to determine the activation of neurons. In training, hyperparameters such as batch size, learning rate, and number of epochs are adjusted to optimize the model. The Adam optimizer (Kingma & Ba, 2015) is employed to update the network parameters and

14678667, 2025, 7, Downloaded from https://onlinelibrary.wiley.com/doi/10.1111/mice.13357 by HONG KONG POLYTECHNIC UNIVERSITY HU NG HOM, Wiley Online Library on [11/03/2025]. See the Terms and Conditions (https://onlinelibrary.wiley.com/terms-and-conditions) on Wiley Online Library for rules of use; OA articles are governed by the applicable Creative Commons License

minimize the mean squared error (MSE) loss function. By minimizing the loss function, the model learns to map input features to accurate regression predictions. Additionally, the model supports training on compute unified device architecture (CUDA)-accelerated graphics processing units (GPUs) to enhance training speed and efficiency. After training, a deep learning model for regression prediction is obtained, which can be utilized as the pre-trained model for subsequent transfer learning tasks.

2.1.4 | Transfer learning model

The transfer learning model is developed by adjusting input parameters and fine-tuning on pre-trained models. Since the NLP data processor and gated transformer can process names and values of parameters into encoded token-level embeddings, even if the new dataset has parameters different from those in the pre-trained model dataset, the pre-trained model can still accept new data that have been processed to encoded embeddings. This allows the pre-trained model to capture the semantic and numerical information contained in the new data, enabling effective fine-tuning on the pre-trained model to greatly improve the possibility and efficiency of model training. By pre-processing the new dataset, updating parameters, and fine-tuning the pre-trained model, the corresponding transfer learning model can be obtained, achieving knowledge transfer in this process.

2.2 | XGBoost

The current state-of-the-art approaches for tabular data modelling are tree-based ensemble methods such as XGBoost technique (T. Chen & Guestrin, 2016). XGBoost surpasses traditional gradient boosting decision trees by supporting various weak learners, employing a more advanced second-order Taylor expansion for loss function simplification, and including a regularization term to prevent overfitting. Its sparsity-aware design and optimized resource allocation also enhance training efficiency, compared to conventional tree models. Notably, the XGBoost framework stands out in sequential training with weak learners and in mitigating overfitting through regularization. Motivated by the proposed research (P.-F. Zhang, Iqbal, et al., 2024), this paper first built an XGBoost model to predict the failure mode of FRP bars embedded in UHPC. Afterward, two XGBoost models were developed for bond strength predictions regarding different failure modes, which serve as references to transfer learning models.

2.3 | Evaluation criterion

To evaluate the performances of bond strength models, three regression criteria are employed as presented in Equations (5)–(7), which are coefficient of determination (R^2), mean absolute error (MAE), and root mean square error (RMSE). Generally, R^2 closer to 1, lower MAE and RMSE indicate better performance. As shown in Equation (8), the classification criterion accuracy is to assess the efficiency of failure mode prediction.

$$R^2 = 1 - \frac{\sum_{i=1}^{n} (\hat{y}_i - y_i)^2}{\sum_{i=1}^{n} (y_i - \bar{y})^2} \tag{5}$$

$$\text{MAE} = \frac{1}{n} \sum_{i=1}^{n} |\hat{y}_i - y_i| \tag{6}$$

$$\text{RMSE} = \sqrt{\frac{1}{n} \sum_{i=1}^{n} (\hat{y}_i - y_i)^2} \tag{7}$$

$$\text{Accuracy} = \frac{\text{TP} + \text{TN}}{\text{TP} + \text{FN} + \text{FP} + \text{TN}} \tag{8}$$

where n is the number of data; y_i and $\hat{y}_i$ are real and predicted values; $\bar{y}$ is the average of real values; TP, TN, FP, and FN are true positive, true negative, false positive, and false negative values, respectively.

The use of multiple fitness and classification criteria, which involves evaluating various metrics on a single problem, helps ensure the robustness of the ML models (Naser & Alavi, 2021). The choice of R^2, MAE, and RMSE as evaluation metrics stems from their complementary roles in capturing different aspects of model performance. R^2 evaluates the goodness of fit and indicates the proportion of variance explained by the model, while MAE and RMSE, though related, measure the average magnitude and overall accuracy of prediction errors, respectively. Moreover, classification accuracy specifically gauges the model's ability to correctly predict distinct failure modes.

3 | DATASET FOR PULLOUT AND BEAM TESTS

3.1 | Pullout test

The pullout test, widely used to evaluate the bond performance between FRP bar and concrete due to its simplicity (Gudonis et al., 2014), involves a concrete cube specimen with an embedded FRP bar fixed inside a testing apparatus capable of applying axial pull forces (Figure 2). Consistent with a previous study (P.-F. Zhang, Iqbal, et al., 2024), this setup includes load and displacement sensors to measure the applied force and the displacement of the FRP

14678667, 2025, 7, Downloaded from https://onlinelibrary.wiley.com/doi/10.1111/mice.13357 by HONG KONG POLYTECHNIC UNIVERSITY HU NG HOM, Wiley Online Library on [11/03/2025]. See the Terms and Conditions (https://onlinelibrary.wiley.com/terms-and-conditions) on Wiley Online Library for rules of use; OA articles are governed by the applicable Creative Commons License

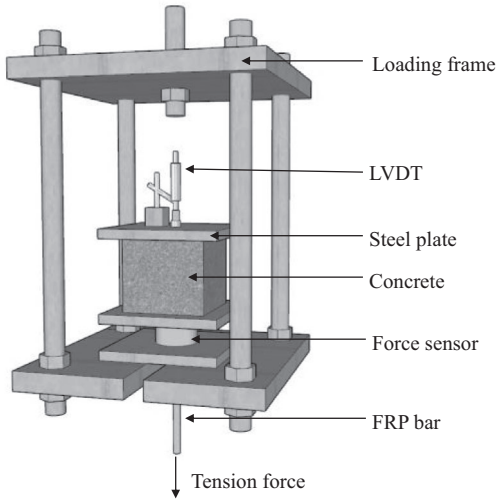

FIGURE 2 Schematic diagram of pullout test setup. LVDT denotes Linear Variable Differential Transformer. (P.-F. Zhang, Iqbal, et al., 2024).

bar. During the test, the FRP bar is gradually pulled out of the concrete by increasing axial forces until bond failure occurs. The bond strength is then calculated using the peak force and the circumferential area of the FRP bar.

3.2 | RILEM beam test

The hinged beam test investigates the bond behavior of FRP bars in UHPC under bending in accordance with the international union of laboratories and experts in construction materials, systems and structures (RILEM) specification (RILEM, 1994). Unlike the direct pullout test, where compressive stress is resisted by concrete and tensile stress by the FRP bar, the hinged beam test subjects both the concrete and the FRP bar to the same tensile stress in the tensile zone (S. J. Yoo et al., 2024). The beam test specimen in the RILEM specification (RILEM, 1994) is shown in Figure 3. The test beam consists of two parallelepipedal reinforced concrete blocks, interconnected at the bottom by the bar whose bond is under investigation and at the top by a steel hinge. The beam is loaded in simple flexure by two forces of equal magnitude, symmetrically disposed regarding the mid-span section of the beam. Finally, the bond strength is calculated according to the specification.

3.3 | Data of pullout and beam tests

This study collected 115 beam test data points (Hossain et al., 2017; Hu et al., 2024; Kauffman & Fam, 2024; Michaud et al., 2021) and 479 pullout test data (see the dataset in P.-F. Zhang, Zhao, et al., 2024) for GFRP bars embedded in. The input attributes include the mechanical properties and constituents of UHPC, as well as the mechanical, geometric, and surface properties of FRP bars. The failure modes were categorized as either pullout failure (1) or concrete splitting failure (2). Typically, pullout failure refers to the gradual extraction of the FRP bar from the concrete until complete separation, with no significant cracks in the concrete; in contrast, splitting failure occurs due to the insufficient tensile resistance of the concrete, leading to longitudinal cracks along the direction of the FRP bar (S. J. Yoo et al., 2024). However, pullout tests primarily subject FRP bars to tensile and concrete to compressive forces, whereas beam tests involve both FRP bars and concrete in tensile stress (ACI Committee 408, 2003). Specifically, the stress distributions (Jeong et al., 2022) and failure modes (real picture—Michaud et al., 2021; Tong et al., 2023, and schematic drawing) for pullout and RILEM beam tests are demonstrated in Figure 4.

In the beam test data, 49 data points correspond to pullout failure, and 66 to concrete splitting failures. Due to the limited amount of beam test data, the distribution of parameters in different failure modes might differ significantly. Descriptive statistical summaries of pullout test data, and beam test data regarding different failure modes are presented in Tables 1–3.

It is important to emphasize that both pullout and beam tests have limitations when it comes to accurately capturing the bond behavior between FRP bars and UHPC as discussed in the Introduction. Additionally, the prediction target in this study is the static bond strength, corresponding to the peak load in bond behavior. However, this metric alone does not fully reflect the complete constitutive relationship of the bond between FRP bars and UHPC.

Specifically, Table 1 was used to develop the pre-trained model, and therefore it was designed to include extensive information on the bond behavior of FRP bars. Detailed explanations of the parameters in Table 1 can be found in the previous study (P.-F. Zhang, Zhao, et al., 2024), with additional notes provided below for the parameters related to the beam test data (Tables 2 and 3).

(1) Polypropylene (PP)/polythene (PE) fibers are used in the specimens of the pullout test, while polyvinyl alcohol (PVA) fibers are used in the beam test.
(2) Only sand-coated GFRP bars are investigated in the beam test. In contrast, the pullout test involves five surface treatment types and three fiber types. Five surface treatment types are labeled as 1, 2, 3, 4, and 5, corresponding to helically wrapped (HW), HW and sand-coated, ribbed, smooth, and sand-coated. Three fiber types of FRP bars—GFRP, basalt FRP, and carbon

14678667, 2025, 7, Downloaded from https://onlinelibrary.wiley.com/doi/10.1111/mice.13357 by HONG KONG POLYTECHNIC UNIVERSITY HU NG HOM, Wiley Online Library on [11/03/2025]. See the Terms and Conditions (https://onlinelibrary.wiley.com/terms-and-conditions) on Wiley Online Library for rules of use; OA articles are governed by the applicable Creative Commons License

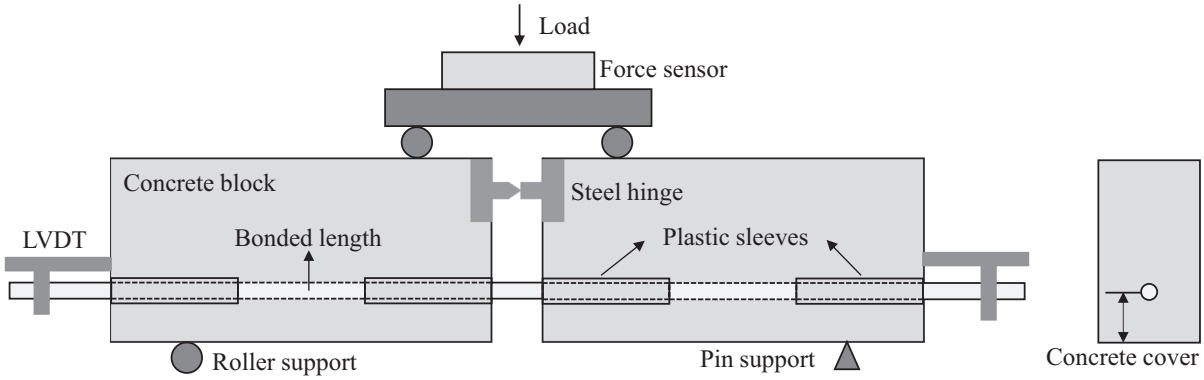

FIGURE 3 Schematic diagram of hinged beam test setup (RILEM, 1994).

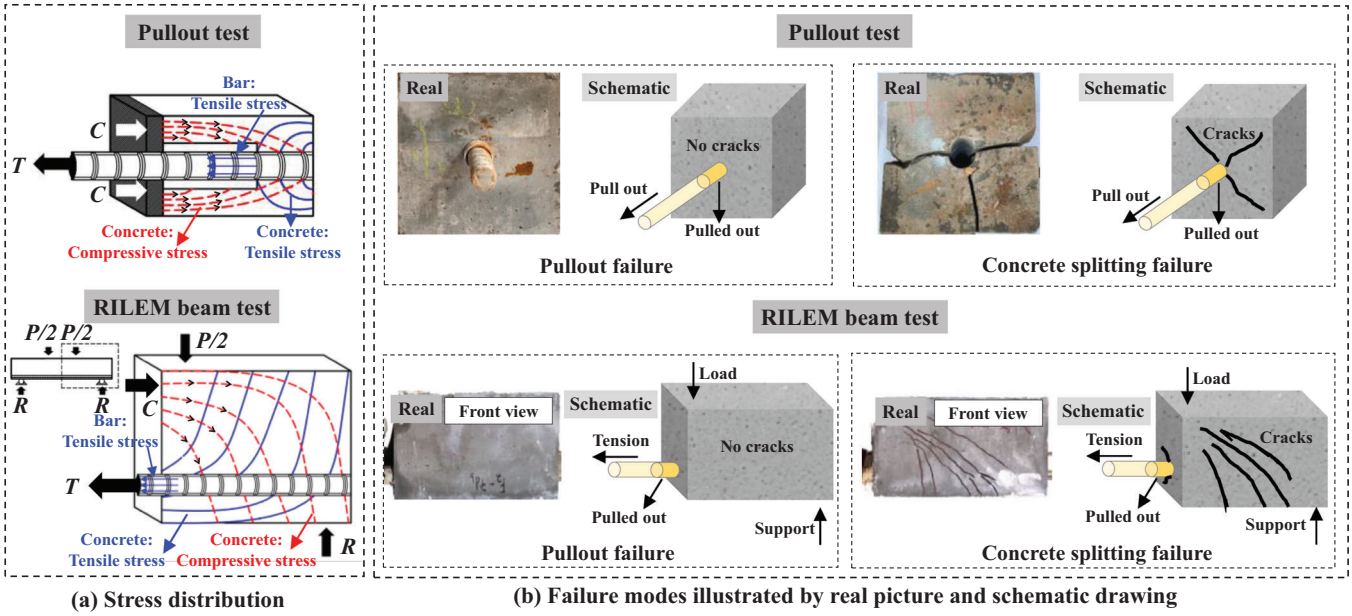

FIGURE 4 Illustration of pullout and RILEM beam tests: (a) Stress distributions (Jeong et al., 2022) and (b) failure modes illustrated by real picture (Michaud et al., 2021; Tong et al., 2023) and schematic drawing.

TABLE 1 Statistics of 479 pullout test data for pullout and concrete splitting failure modes.

	Parameter	Mean	Min	Max	Std	Skewness	Kurtosis
Input	Vf of steel fiber	1.70	0.00	3.00	0.75	−1.53	1.15
	Vf of PP/PE fiber	0.09	0.00	1.00	0.28	2.97	6.86
	Concrete compressive strength (MPa)s	152.63	90.10	201.80	30.34	−0.13	−1.22
	Water-to-binder ratio	0.18	0.12	0.24	0.03	0.43	−0.65
	Sand-to-binder ratio	1.06	0.69	1.31	0.18	−0.22	−1.11
	Bar diameter (mm)	15.87	6.00	22.00	3.76	−0.56	−0.59
	Cover-to-diameter ratio	4.41	0.50	16.70	3.04	1.62	3.24
	Bonded-length-to-diameter ratio	3.86	1.00	10.00	2.17	0.59	−0.20
	Rib-spacing-to-diameter ratio	0.46	0.00	2.50	0.48	1.50	3.68
	Rib-height-to-diameter ratio	3.58	0.00	13.30	3.88	0.59	−0.77
	Bar surface treatment	/	/	/	/	/	/
	Bar fiber type	/	/	/	/	/	/
	Bar tensile elastic modulus (GPa)	57.56	41.00	127.00	16.20	3.06	9.77
	Failure mode	/	/	/	/	/	/
Output	Bond strength (MPa)	23.88	6.30	56.24	11.05	0.98	0.58

14678667, 2025, 7, Downloaded from https://onlinelibrary.wiley.com/doi/10.1111/mice.13357 by HONG KONG POLYTECHNIC UNIVERSITY HU NG HOM, Wiley Online Library on [11/03/2025]. See the Terms and Conditions (https://onlinelibrary.wiley.com/terms-and-conditions) on Wiley Online Library for rules of use; OA articles are governed by the applicable Creative Commons License

TABLE 2 Statistics of 49 beam test data for pullout failure.

	Parameter	Mean	Min	Max	Std	Skewness	Kurtosis
Input	Vf of steel fiber	2.00	2.00	2.00	0.00	/	/
	Vf of PVA fiber	0.00	0.00	0.00	0.00	/	/
	Concrete compressive strength (MPa)	150.84	118.00	174.50	18.24	−0.12	−1.25
	Bar diameter (mm)	17.05	13.50	19.10	1.68	0.12	−1.17
	Cover-to-diameter ratio	2.76	2.00	3.70	0.46	−0.26	−0.54
	Bonded-length-to-diameter ratio	5.10	2.50	10.00	2.00	0.74	0.17
	Rib-spacing-to-diameter ratio	0.00	0.00	0.00	0.00	/	/
	Rib-height-to-diameter ratio	0.00	0.00	0.00	0.00	/	/
	Bar tensile elastic modulus (GPa)	56.00	47.60	64.10	7.09	−0.04	−1.83
Output	Bond strength (MPa)	20.65	10.90	30.41	5.03	0.25	−0.58

TABLE 3 Statistics of 66 beam test data for concrete splitting failure.

	Parameter	Mean	Min	Max	Std	Skewness	Kurtosis
Input	Vf of steel fiber	1.79	0.00	4.00	1.12	−0.04	0.23
	Vf of PVA fiber	0.53	0.00	3.00	1.06	1.62	0.89
	Concrete compressive strength (MPa)	120.83	87.00	146.00	15.84	−1.00	0.07
	Bar diameter (mm)	18.45	13.50	27.00	4.27	1.27	0.41
	Cover-to-diameter ratio	1.75	1.00	3.60	0.60	1.96	3.34
	Bonded-length-to-diameter ratio	9.94	4.00	16.00	3.86	−0.20	−1.13
	Rib-spacing-to-diameter ratio	0.00	0.00	0.00	0.00	/	/
	Rib-height-to-diameter ratio	0.00	0.00	0.00	0.00	/	/
	Bar tensile elastic modulus (GPa)	62.22	62.00	62.70	0.25	0.99	−0.31
Output	Bond strength (MPa)	14.44	5.90	28.50	4.96	0.51	0.06

FRP—are denoted by 1, 2, and 3, respectively. Based on the previous study, the influences of fiber type and surface treatment were reflected by the bar tensile elastic modulus, rib-spacing-to-diameter ratio, and rib-height-to-diameter ratio (P.-F. Zhang, Iqbal, et al., 2024; P.-F. Zhang, Zhao, et al., 2024). Thus, these three parameters were used to represent the sand-coated surface and glass fiber type.

Additionally, the parametric distribution histograms with overlaid normal distribution curves for both pullout and beam test data are presented in Figures 5 and 6. Figure 5 illustrates the distribution of parameters from the pullout test data as shown in Table 1, while Figure 6 highlights the distribution of beam test parameters from Tables 2 and 3, distinguishing between pullout and concrete splitting failures. Notably, Figure 6 excludes the rib-spacing-to-diameter ratio and rib-height-to-diameter ratio as their values are zero. It can be observed that for the parameters in Tables 1–3, the data are predominantly distributed within a continuous range, with few outliers. This distribution provides a robust foundation for the development of both pre-trained and transfer learning models.

4 | DEVELOPMENT OF TRANSFER LEARNING MODELS ON BOND STRENGTH PREDICTION

The workflow to predict the beam test bond strength of FRP bars in UHPC is illustrated in Figure 7. First, the parameters of the beam test are input into the XGBoost-failure mode (FM) prediction model to classify the FM. Once the FM is determined, input parameters are fed into the corresponding transfer learning (TL), XGBoost, and NN models to predict the bond strength (BS) in case of concrete splitting failure (SF) or pullout failure (PF). The modeling approaches of the XGBoost-FM prediction model, TL bond strength prediction models, and XGBoost and NN bond strength prediction models are presented in the following sections.

4.1 | XGBoost-FM prediction model

The workflow of the FM prediction model is shown in Figure 8. The output parameter, failure mode, was

14678667, 2025, 7, Downloaded from https://onlinelibrary.wiley.com/doi/10.1111/mice.13357 by HONG KONG POLYTECHNIC UNIVERSITY HU NG HOM, Wiley Online Library on [11/03/2025]. See the Terms and Conditions (https://onlinelibrary.wiley.com/terms-and-conditions) on Wiley Online Library for rules of use; OA articles are governed by the applicable Creative Commons License

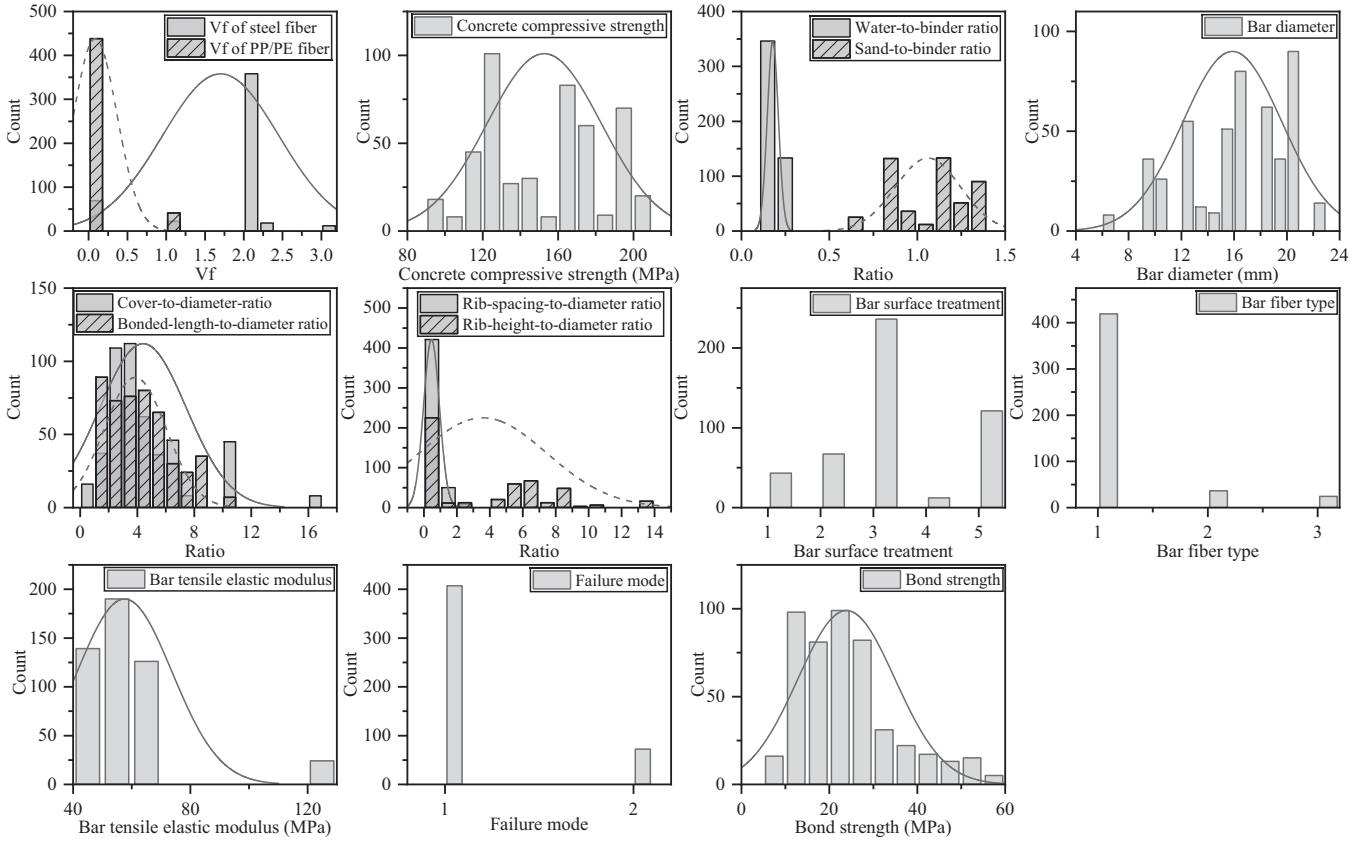

FIGURE 5 Parametric distribution of pullout test data.

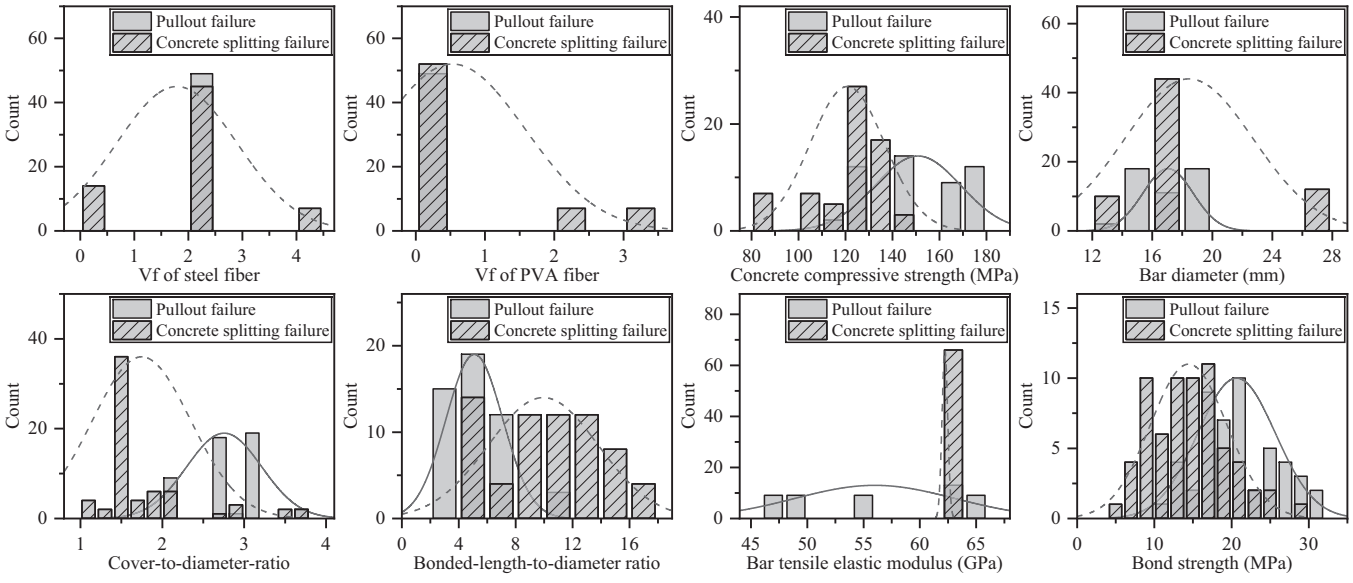

FIGURE 6 Parametric distribution of beam test data regarding pullout and concrete splitting failure modes.

categorized as either pullout failure (1) or concrete splitting failure (2). Initially, the data were randomly split into a training set and a testing set with an empirical ratio of 8:2. The input parameters were standardized using Equation (9), ensuring that all parameters had zero mean and unit variance after standardization.

$$X_{\text{stand}} = \frac{X - \mu}{\sqrt{\sigma^2}} \tag{9}$$

14678667, 2025, 7, Downloaded from https://onlinelibrary.wiley.com/doi/10.1111/mice.13357 by HONG KONG POLYTECHNIC UNIVERSITY HU NG HOM, Wiley Online Library on [11/03/2025]. See the Terms and Conditions (https://onlinelibrary.wiley.com/terms-and-conditions) on Wiley Online Library for rules of use; OA articles are governed by the applicable Creative Commons License

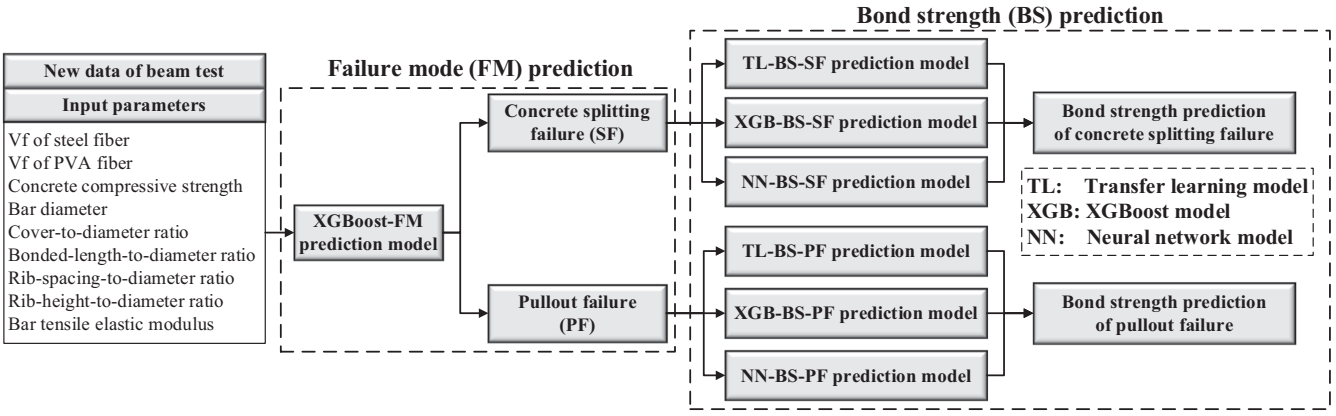

FIGURE 7 Workflow to predict the failure modes and bond strength using beam test data.

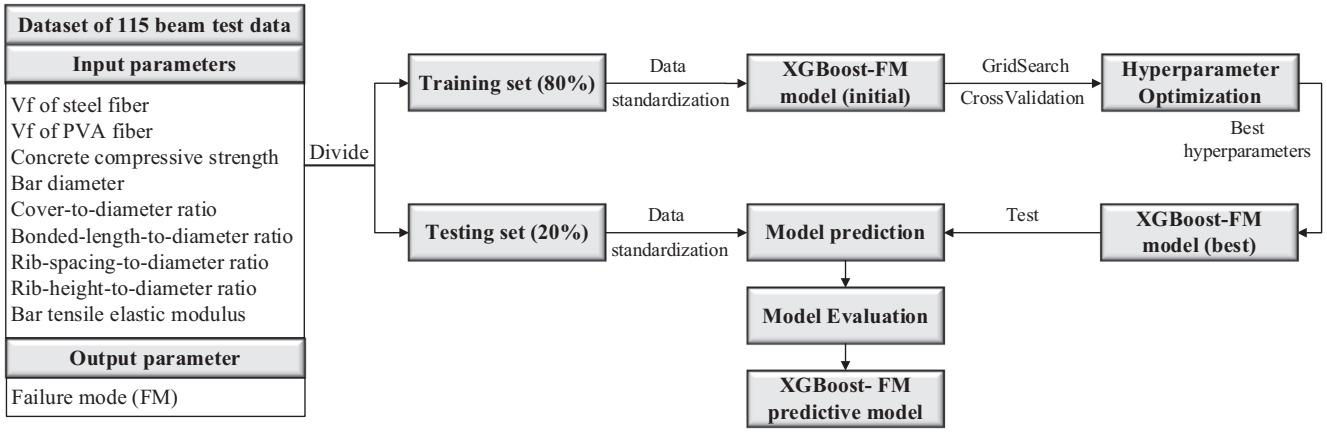

FIGURE 8 Workflow of the XGBoost-FM prediction model.

where X is the data of each input parameter; μ and σ are the mean value and variance of data, respectively.

To maintain consistency in the distribution of the testing set with the training set, the testing set was standardized using the mean value and variance of the training set (P.-F. Zhang, Iqbal, et al., 2024). After data processing, the XGBoost prediction model for FM was trained. It is important to emphasize that hyperparameters, which are inherent to models and must be manually set, have a direct impact on model performance. To achieve the ideal models, the optimal combination of hyperparameters was determined using the GridSearchCV method, which has been proven effective in the previous study (P.-F. Zhang, Iqbal, et al., 2024). GridSearchCV is an automated parameter tuning technique that evaluates different hyperparameter combinations through k-fold cross-validation based on specific evaluation criteria. The hyperparameter choice of "n_estimators", "max_depth", "learning_rate" and "booster" aims to optimize the XGBoost model's performance. "n_estimators" determines the number of base learners in the ensemble, and when combined with "learning_rate," balances model complexity and generalization. "max_depth" controls each tree's complexity, ensuring adequate feature interaction capture while preventing overfitting. The "booster" parameter enables the selection of the most suitable base model for the data and task, enhancing the model's flexibility and accuracy. Adjusting these key parameters refines the model's learning ability and mitigates overfitting. The optimal hyperparameters for the XGBoost-FM prediction model are presented in Table 4, where optimal values correspond to the highest R^2 score among hyperparameter grids during the process of hyperparameter optimization.

4.2 | Transfer learning bond strength prediction models

As illustrated in Figure 9, the TL model for bond strength prediction was developed using the proposed TransTabRegressor framework (Figure 1) in Section 2.1. The left part

14678667, 2025, 7, Downloaded from https://onlinelibrary.wiley.com/doi/10.1111/mice.13357 by HONG KONG POLYTECHNIC UNIVERSITY HU NG HOM, Wiley Online Library on [11/03/2025]. See the Terms and Conditions (https://onlinelibrary.wiley.com/terms-and-conditions) on Wiley Online Library for rules of use; OA articles are governed by the applicable Creative Commons License

TABLE 4 Optimal hyperparameters of the XGBoost-FM model.

Hyperparameters	Initial value	[Test range] (Increment size)	Optimal value
n_estimators	100	[10, 200] (10)	20
max_depth	None	[1, 20] (1)	4
learning_rate	0.3	0.3	0.3
booster	gbtree	[gbtree, gblinear, dart]	gbtree

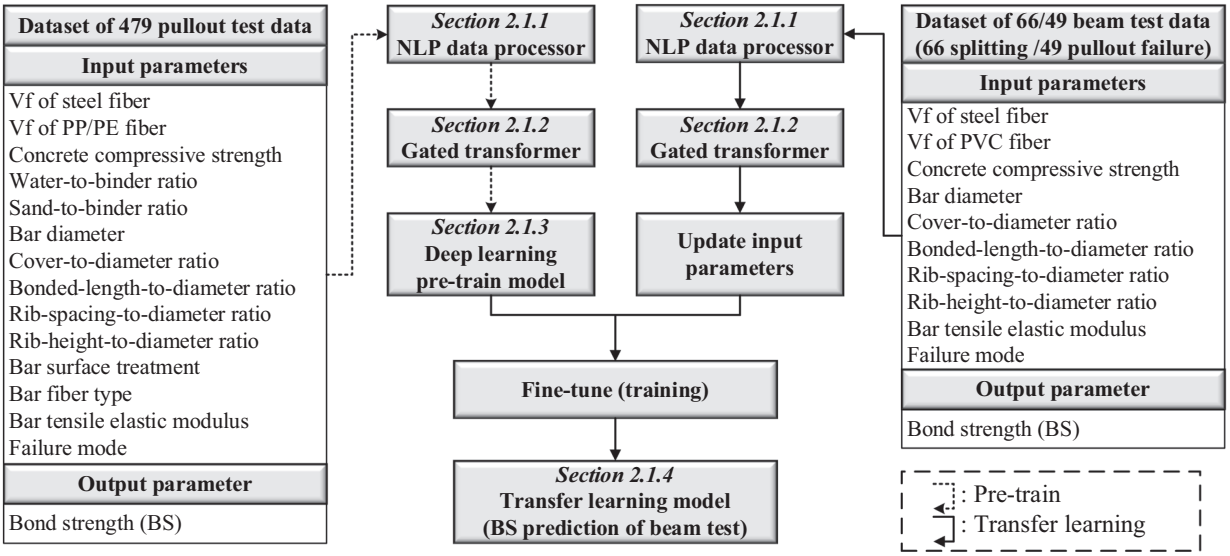

FIGURE 9 Workflow of transfer learning using TransTabRegressor framework.

of Figure 9 showcases the pre-trained model, which was trained on a diverse dataset of 479 pullout tests considering 14 parameters. This model captures the general patterns and features of the bond mechanism between FRP bars and UHPC, serving as a foundational starting point. The right part of Figure 9 demonstrates how the TL model was fine-tuned using 115 beam test data points (66 for SF and 49 for PF), enabling the model to leverage the learned representations without requiring training from scratch.

The modeling process of the pre-trained model (left part of Figure 9) is outlined as follows, which serves as a precursor to developing the TL model.

First, the NLP data processor module described in Section 2.1.1 was employed to process the data. This involved tokenizing the data and matching it to the token embedding matrix using the BERT tokenizer (Devlin et al., 2019). The names of the input parameters were converted into 16-dimensional embeddings through a vocabulary embedding layer with a size of 30,522. Each token was represented as a 16-dimensional vector, which was then multiplied by the parameter value to obtain the input data embedding. The output parameter underwent a similar process. Following this, layer normalization was applied to align the input and output parameter embeddings, both set to 16 dimensions, via an alignment layer.

Next, the gated transformer module from Section 2.1.2 was utilized to further process the data. This module, comprising multiple layers, including a multi-head self-attention layer, gated feedforward layers, and layer normalization, enabled the model to capture complex relationships among input parameters and enhance parameter representation. Specifically, two layers of gated transformers were used, with the hidden dimension of intermediate dense layers set to 256 and the attention module featuring eight heads. In the final stage of the encoder, a special token for parameter aggregation was used to consolidate all input parameters, helping the model capture the semantic information of the entire tabular data and providing a global parameter representation for subsequent regression tasks.

Finally, the deep learning module in Section 2.1.3 was used to build the pre-trained model. A regression NN was trained to predict bond strength. Initially, the data were randomly split into a training set and a testing set with an 8:2 ratio. The Adam optimizer and MSE loss function were employed to update the model parameters. A hyperparameter grid was set up to identify the

14678667, 2025, 7, Downloaded from https://onlinelibrary.wiley.com/doi/10.1111/mice.13357 by HONG KONG POLYTECHNIC UNIVERSITY HU NG HOM, Wiley Online Library on [11/03/2025]. See the Terms and Conditions (https://onlinelibrary.wiley.com/terms-and-conditions) on Wiley Online Library for rules of use; OA articles are governed by the applicable Creative Commons License

TABLE 5 Optimal hyperparameters of the pre-trained model.

Hyperparameters	[Set range] (Increment size)	Optimal value
hidden_layer	[1, 2]	1
hidden_dimension	[20, 40, 60, 80, (20,20), (40,40), (60,60)]	40
batch_size	[50, 100, 150, 200]	100
num_epoch	[50, 200] (10)	100
learning_rate	[0.1, 0.01, 0.001, 0.0001]	0.01

TABLE 6 Optimal hyperparameters of TL models.

Failure mode	Hyperparameters	[Set range] (Increment size)	Optimal value
SF	batch_size	[20, 30,40, 50]	40
	num_epoch	[50, 200] (2)	100
	learning_rate	[0.1, 0.01, 0.001, 0.0001]	0.01
PF	batch_size	[10, 20, 30, 40]	30
	num_epoch	[50, 120] (2)	102
	learning_rate	[0.1, 0.01, 0.001, 0.0001]	0.01

optimal hyperparameters, including the number of hidden layers (hidden_layer), the dimension of hidden layers (hidden_dimension), batch size (batch_size), number of epochs (num_epoch), and learning rate (learning_rate), as shown in Table 5. Through this process, the optimal hyperparameters were identified as presented in Table 5. In detail, the ideal pre-trained regression model for bond strength prediction consisted of three layers. The first layer had an input dimension of 16, determined by the embedding dimension of the input parameters. The second layer had a hidden dimension of 40, and the third layer had a dimension of 1 for output, yielding the final bond strength predictions. This model served as the pre-trained model for subsequent TL module to derive the beam test bond strength prediction model.

Subsequently, the TL models for beam test bond strength were established by fine-tuning the pre-trained model using the TL module described in Section 2.1.4. A total of 66 data points for SF and 49 data points for PF were used to develop models for the respective FMs. As shown in the right part of Figure 9, the input data were pre-processed by the NLP data processor and gated transformer similar to the pre-trained model. After processing, the input parameters were updated to account for the differences between the beam test data and the pullout test data. The TL models were then built by fine-tuning the pre-trained model. Notably, the TL models share the same structure as the pre-trained model, meaning that only the weights between layers needed to be re-trained. The optimal hyperparameters for the TL models of concrete splitting and PF are listed in Table 6.

4.3 | XGBoost and NN bond strength prediction models

The XGBoost and NN models for bond strength prediction regarding different FMs were directly trained on the beam test data, with 66 data points for SF and 49 data points for PF. For comparison with the TL models, the NN models were also trained with the same network structure (16, 40, 1) based on the TransTabRegressor framework. The XGBoost modeling procedures were similar to the developed model in Section 4.1, and the optimal hyperparameters for the XGBoost and NN models are presented in Tables 7 and 8.

5 | RESULTS AND DISCUSSION

5.1 | Evaluation of FM prediction

The dataset included two FMs: pullout failure (1) and concrete splitting failure (2). Using a threshold of 1.5, predicted values below this threshold were classified as PF, while those above were classified as SF. The FM predicted results of the XGBoost model are presented in Figure 10. Notably, all prediction errors were within the range of 0.02, indicating that the FMs were predicted with high accuracy. The model achieved an accuracy of 100%, calculated using Equation (8). As shown in Figure 5, the XGBoost-FM model can effectively predict FMs based on the input parameters of beam test data. This accurate prediction facilitates further forecasting of bond strength associated with different FMs.

14678667, 2025, 7, Downloaded from https://onlinelibrary.wiley.com/doi/10.1111/mice.13357 by HONG KONG POLYTECHNIC UNIVERSITY HU NG HOM, Wiley Online Library on [11/03/2025]. See the Terms and Conditions (https://onlinelibrary.wiley.com/terms-and-conditions) on Wiley Online Library for rules of use; OA articles are governed by the applicable Creative Commons License

TABLE 7 Optimal hyperparameters of XGBoost-BS models.

Failure mode	Hyperparameters	Initial value	[test range] (Increment size)	Optimal value
SF	n_estimators	100	[10, 200] (10)	60
	max_depth	None	[1, 20] (1)	6
	subsample	1	[1, 0.8, 0.6]	1
	learning_rate	0.3	0.3	0.3
	booster	gbtree	[gbtree, gblinear, dart]	gbtree
Pullout failure	n_estimators	100	[10, 200] (10)	50
	max_depth	None	[1, 20] (1)	6
	Subsample	1	[1, 0.8, 0.6]	1
	learning_rate	0.3	0.3	0.3
	Booster	gbtree	[gbtree, gblinear, dart]	gbtree

TABLE 8 Optimal hyperparameters of NN-BS models.

Failure mode	Hyperparameters	[Set range] (increment size)	Optimal value
SF	batch_size	[20, 30,40, 50]	40
	num_epoch	[50, 200] (2)	100
	learning_rate	[0.1, 0.01, 0.001]	0.01
PF	batch_size	[10, 20, 30, 40]	30
	num_epoch	[50, 150] (2)	90
	learning_rate	[0.1, 0.01, 0.001]	0.01

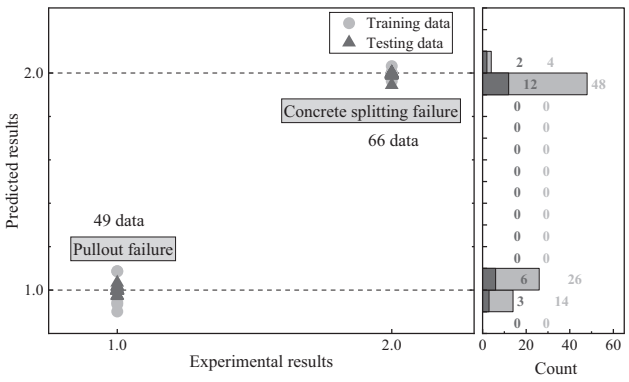

FIGURE 10 Evaluation of the XGBoost-FM prediction model.

5.2 | Comparison of transfer learning to other models on bond strength prediction

As discussed in the modeling chapter, the XGBoost and NN models were directly trained on 66 data points in case of SF and 49 data points of PF. However, the TL model was fine-tuned on a pre-trained model developed using 479 data points from pullout tests, utilizing the same beam test data. The evaluation metrics for the bond strength prediction models regarding concrete splitting and PF are summarized in Tables 9 and 10. Additionally, the bond strength prediction distributions of different models for two FMs are presented in Figures 11 and 12.

In summary, the TL models showed higher R^2 and lower MAE and RMSE values, compared to XGBoost and NN models. Besides, the precise prediction performances of the TL models based on the excellent statistical indices highlighted the consistency of the dataset (Gribniak et al., 2015). And the detailed analysis of prediction evaluation regarding different FMs is presented below.

5.2.1 | Bond strength in case of concrete splitting failure

The bond strength prediction distributions of different models for SF are presented in Figure 11. As shown in Table 9, the XGBoost model performs exceptionally well on the training set with an R^2 of 0.995 but shows overfitting with a significant drop in testing performance (R^2: 0.899; MAE: 1.156; RMSE: 1.589). The NN model also performs well during training (R^2: 0.977, MAE: 0.562; RMSE: 0.735), but their testing performance is slightly lower (R^2: 0.887; MAE: 1.315; RMSE: 1.763), indicating moderate overfitting. The TL model stands out with consistent performance across both training and testing sets. Despite performing well on the training set with an R^2 of 0.980, it achieves a high R^2 (0.975) on the testing set, with significantly lower MAE (0.632) and RMSE (0.829), compared to the other

14678667, 2025, 7, Downloaded from https://onlinelibrary.wiley.com/doi/10.1111/mice.13357 by HONG KONG POLYTECHNIC UNIVERSITY HU NG HOM, Wiley Online Library on [11/03/2025]. See the Terms and Conditions (https://onlinelibrary.wiley.com/terms-and-conditions) on Wiley Online Library for rules of use; OA articles are governed by the applicable Creative Commons License

TABLE 9 Indices evaluation of bond strength prediction models for concrete splitting failure.

	Coefficient of determination (R^2)		Mean Absolute Error (MAE)		Root Mean Square Error (RMSE)	
	Training set	Testing set	Training set	Testing set	Training set	Testing set
XGBOOST	0.995	0.899	0.127	1.156	0.356	1.589
NN	0.977	0.887	0.562	1.315	0.735	1.763
TL	0.980	0.975	0.498	0.632	0.683	0.829

TABLE 10 Indices evaluation of bond strength prediction models for pullout failure.

	R^2		MAE		RMSE	
	Training set	Testing set	Training set	Testing set	Training set	Testing set
XGBoost	0.999	0.851	0.071	1.249	0.191	1.533
NN	0.972	0.849	0.578	1.622	0.829	1.876
TL	0.982	0.955	0.486	0.840	0.665	0.969

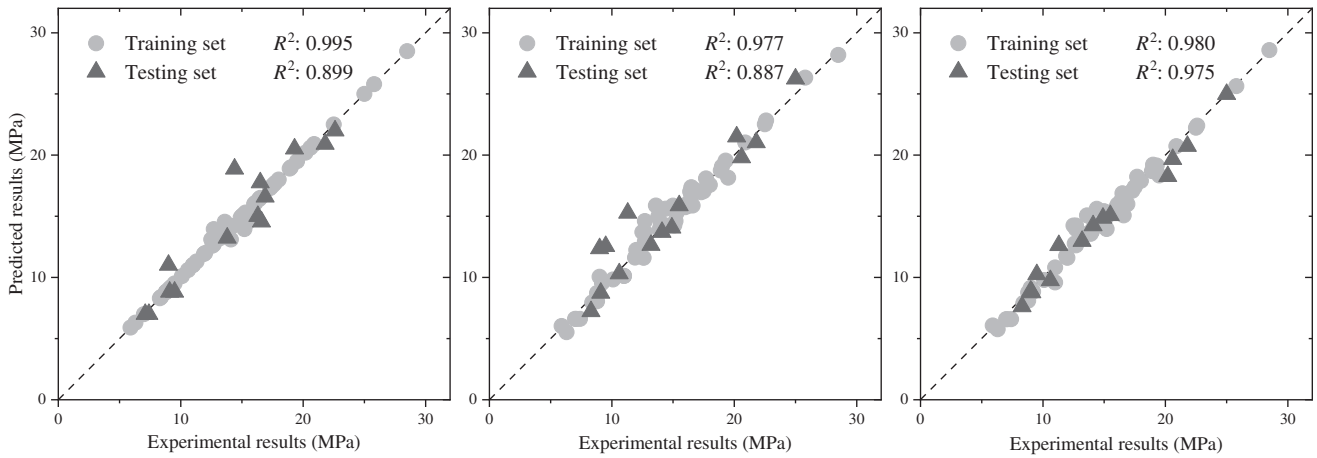

(1) XGBoost model (2) NN model (3) Transfer learning model

FIGURE 11 Prediction distribution of bond strength prediction models for concrete splitting failure.

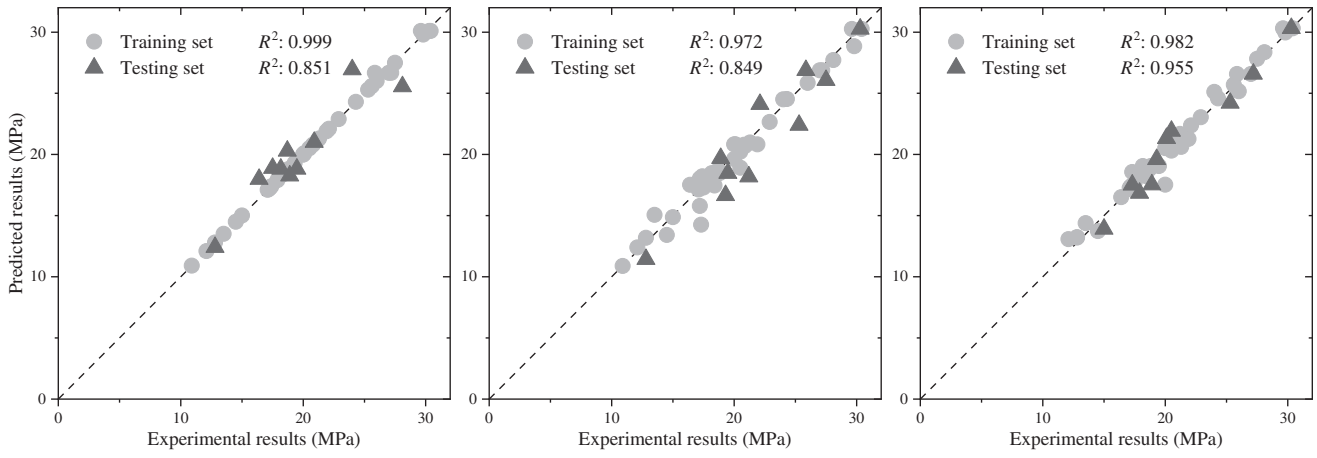

(1) XGBoost model (2) NN model (3) Transfer learning model

FIGURE 12 Prediction distribution of bond strength prediction models for pullout failure.

14678667, 2025, 7, Downloaded from https://onlinelibrary.wiley.com/doi/10.1111/mice.13357 by HONG KONG POLYTECHNIC UNIVERSITY HU NG HOM, Wiley Online Library on [11/03/2025]. See the Terms and Conditions (https://onlinelibrary.wiley.com/terms-and-conditions) on Wiley Online Library for rules of use; OA articles are governed by the applicable Creative Commons License

models, indicating robust generalization and reliable predictions.

Specifically, the MAE (0.632) and RMSE (0.829) values of the TL model showed significantly low average predicted errors of 4.38% and 5.74%, compared to the average bond strength of 14.44 MPa for the testing data, respectively (Avg. bond strength value taken from Table 3). While those errors of MAE and RMSE were (8.00%, 13.09%) and (9.11%, 12.21%) for testing data of XGBoost and NN models. The excellent evaluation indices of R^2, MAE, and RMSE verified the consistency and effectiveness of data in case of SF. Compared to the directly trained XGBoost and NN models, the prediction accuracy and robustness in generalization make the TL model a highly effective approach for this prediction task on bond strength in case of SF.

5.2.2 | Bond strength of pullout failure

The bond strength prediction distributions of different models for PF are presented in Figure 12. As shown in Table 10, in predicting PF, the XGBoost model shows extreme overfitting, with near-perfect performance on the training set (R^2: 0.999; MAE: 0.071; RMSE: 0.191) but a substantial drop on the testing set (R^2: 0.851; MAE: 1.249; RMSE: 1.533). The NN model exhibits better generalization than XGBoost but still shows a noticeable performance drop between training and testing sets. TL proves to be the most effective model for predicting bond strength in PF. Although it does not achieve the highest R^2 or the lowest errors on the training set, its performance on the testing set is markedly better. With an R^2 of 0.955, it explains a substantial portion of the variance in the testing data, and the relatively low MAE (0.840) and RMSE (0.969) values indicate more accurate and reliable predictions.

Moreover, the MAE (0.840) and RMSE (0.969) values of the TL model showed significantly low average predicted errors of 4.07% and 4.69%, compared to the average bond strength of 20.65 MPa for the testing data, respectively (Avg. bond strength value taken from Table 2), while those errors of MAE and RMSE were (6.05%, 7.85%) and (7.42%, 9.08%) for testing data of XGBoost and NN models. The excellent evaluation indices of R^2, MAE, and RMSE verified the consistency and effectiveness of data of PF. In summary, the TL is less prone to overfitting compared to XGBoost and NNs, making it the most robust and generalizable model for this prediction task.

5.2.3 | Comparative analysis of failure modes

The comparative analysis of the two FMs highlights key differences. In SF, TL significantly outperforms XGBoost and NN on the testing set, demonstrating strong generalization. For PF, while TL also outperforms the other models, its advantage is less pronounced compared to SF. XGBoost shows extreme overfitting in both FMs, with near-perfect training performance but substantial drops in testing performance. NN exhibits moderate overfitting, with decent training performance but noticeable drops in testing performance. TL shows minimal overfitting, maintaining high performance across both training and testing sets. Additionally, MAE and RMSE values are higher for PF, compared to SF, suggesting that predicting bond strength in PF is more challenging. Overall, TL proves to be the most effective and robust model for both FMs, with strong generalization and low errors on testing sets, indicating that PF presents more prediction challenges and may require more sophisticated modeling techniques or additional data preprocessing to improve performance.

5.2.4 | Comparison with ACI code equation

The bond strength between FRP bars and concrete is provided in American concrete institute (ACI) code ACI 440.1R-15 (ACI Committee 440, 2015) using Equation (10), derived from regression analysis based on 67 beam tests in which concrete exhibited SF (Wambeke & Shield, 2006).

$$\frac{\tau_b}{0.083\sqrt{f_c'}} = 4.0 + 0.3\frac{c}{d_b} + 100\frac{d_b}{l_b} \tag{10}$$

where τ_b represents the bond strength (MPa); f_c' denotes the 28-day concrete compressive strength (MPa); c is the lesser of the cover to the center of the bar; d_b is bar diameter; and l_b is the bonded length.

As shown in Table 9, the TL model for predicting the bond strength in cases of SF exhibited high R^2 values, with 0.980 for training data and 0.975 for testing data. The 66 beam test data points in case of SF were used to compare the bond strength prediction capability of the TL model with that of the ACI equation (Equation 10).

The comparison between the predictions of the TL model and Equation (10) in relation to concrete compressive strength is presented in Figure 13. The results indicate that the TL model closely matched the experimental values, achieving a high R^2 value of 0.979. In contrast, the ACI code predictions showed considerable deviation, with a negative R^2. This discrepancy arises because Equation (10) primarily considers only three parameters, while other important factors (listed in Table 3) also significantly influence bond strength. Additionally, Equation (10) was developed using data with compressive strengths ranging from 28 to 45 MPa, whereas the compressive strength in this dataset ranges from 87 to 146 MPa, resulting in a

14678667, 2025, 7, Downloaded from https://onlinelibrary.wiley.com/doi/10.1111/mice.13357 by HONG KONG POLYTECHNIC UNIVERSITY HU NG HOM, Wiley Online Library on [11/03/2025]. See the Terms and Conditions (https://onlinelibrary.wiley.com/terms-and-conditions) on Wiley Online Library for rules of use; OA articles are governed by the applicable Creative Commons License

TABLE 11 Indices evaluation of bond strength prediction models for concrete splitting and pullout failures.

	R^2		MAE		RMSE	
	Training set	**Testing set**	**Training set**	**Testing set**	**Training set**	**Testing set**
Pre-trained model	0.976	0.951	1.326	1.965	1.700	2.539
TL-SF model	0.980	0.975	0.498	0.632	0.683	0.829
TL-PF model	0.982	0.955	0.486	0.840	0.665	0.969

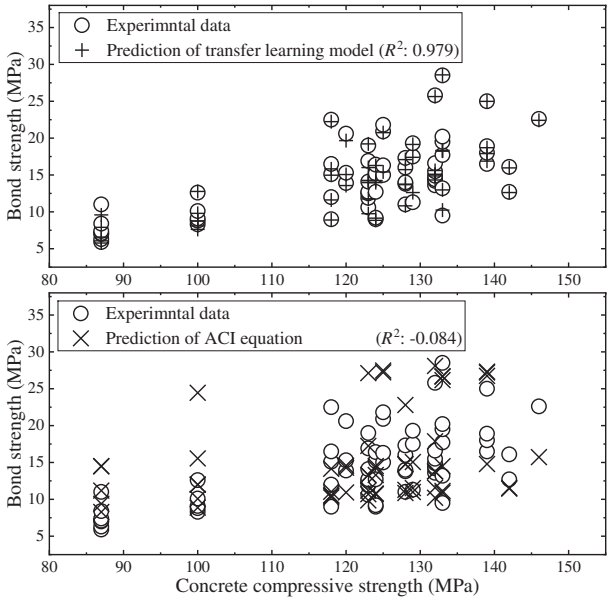

FIGURE 13 Comparison between predictions of transfer learning model and ACI code equation.

substantial overestimation of bond strength by the ACI equation. Furthermore, the TL model was fine-tuned using a large pullout test dataset, enabling it to incorporate more information about bond behavior.

In summary, the TL predictive model outperformed Equation (10), which is limited by the number and range of parameters it considers for determining bond strength, potentially leading to significant deviations.

5.3 | Transferable ability from pullout to beam test data

As discussed in Sections 5.2.1 and 5.2.2, the TL models demonstrated the highest efficiency in predicting bond strength from beam test data. This performance significantly relied on the pre-trained model. In this study, the pre-training was based on 479 data points from pullout tests, utilizing the TransTabRegressor framework. The performances of the pre-trained model and TL models are summarized in Table 11, with SF referring to concrete splitting failure and PF to pullout failure.

The high R^2 values indicate that the pre-trained model was effectively established using the 479 pullout test data points, providing a strong foundation for TL from pullout tests to beam tests. Besides, the MAE (1.965) and RMSE (2.539) values of the pre-trained model showed significantly low average predicted errors of 8.23% and 10.63%, compared to the average bond strength of 23.88 MPa for the testing data, respectively (Avg. bond strength value taken from Table 1). It fully verified the consistency of data for the pre-trained model. As illustrated in Figure 9, the pre-trained model was trained with 14 input parameters from pullout tests, comprehensively considering the mechanical properties and constituents of UHPC, as well as the mechanical, geometric, and surface properties of FRP bars. This allowed the pre-trained model to fully learn and represent the bond behavior of FRP bars in UHPC.

However, only 10 relevant input parameters were available for the beam test, causing a structural change in the data. Conventional ML models struggle with TL due to the need for consistency in data dimensions of input parameters. The proposed TransTabRegressor framework overcame this challenge by converting both the names and values of input parameters into tokens and embeddings, enabling the inclusion of all information in model training. By updating the weights within the network structure of the pre-trained model, the new input parameters can be trained to build the bond prediction models for the beam test.

Unlike traditional ML models such as XGBoost and NNs as comparisons in the manuscript, which rely heavily on the consistency of input dimensions and struggle with variable input structures, TransTabRegressor excels in handling the variations in input parameters between different datasets. For instance, XGBoost and NN require manual feature engineering to align the input dimensions, often leading to information loss or the need for extensive preprocessing. In contrast, TransTabRegressor automatically adjusts to these changes by converting input names and values into embeddings, effectively capturing the full scope of the available data without requiring dimensional consistency. This adaptability significantly enhances its applicability in real-world scenarios where input parameters may vary across datasets.

Additionally, as shown in Tables 2 and 3, some input parameters of the beam test data are constant, which typically do not affect NN training since they do not influence weight updates. However, it was found that adding

14678667, 2025, 7, Downloaded from https://onlinelibrary.wiley.com/doi/10.1111/mice.13357 by HONG KONG POLYTECHNIC UNIVERSITY HU NG HOM, Wiley Online Library on [11/03/2025]. See the Terms and Conditions (https://onlinelibrary.wiley.com/terms-and-conditions) on Wiley Online Library for rules of use; OA articles are governed by the applicable Creative Commons License

several constant parameters improved prediction efficiency. For instance, the rib-height-to-diameter ratio and rib-spacing-to-diameter ratio were both zero but experimentally proved to enhance the model's performance. This effect can be explained by the addition of these parameters altering the data dimension, potentially making it more suitable for specific modeling tasks. Although these constant parameters do not directly affect weight updates, their inclusion increases the dimensionality of the data and changes the feature representation in high-dimensional space, which can help the model capture specific patterns or relationships more effectively. Furthermore, the introduction of constant parameters can influence the distribution of weights in the hidden layers during initialization, affecting the network's learning path or optimization direction, thus improving performance. This occurs because the presence of these parameters modifies the initialization space, potentially guiding the learning process toward more relevant features. Additionally, even though these parameters are numerically zero, they carry useful prior information, such as indicating whether the FRP bars were sand-coated or smooth. This prior knowledge aids the model in better understanding and distinguishing between different input features, which can enhance prediction accuracy. Moreover, it is important to mention that the rib-height-to-diameter ratio and rib-spacing-to-diameter ratio are not suitable for characterizing smooth and sand-coated surfaces, as these surfaces do not have ribs.

Moreover, it is important to address the potential biases in the datasets used. The input parameters for the pullout test data (Table 1) and the beam test data (Tables 2 and 3) differ, which may lead to discrepancies in model performance. For example, the beam test dataset lacks certain parameters such as water-to-binder ratio and sand-to-binder ratio, which are present in the pullout test data but may indirectly influence bonding characteristics. Additionally, variations in experimental conditions and stress states between the pullout and beam tests may result in different effects of the same input parameters on bond strength. For instance, parameters such as bar diameter and cover thickness may have varying effects due to these differing test conditions. Furthermore, different failure mechanisms and deformation measurement errors can introduce additional biases, affecting prediction accuracy. These factors underscore the need for careful consideration of dataset characteristics and potential biases to ensure reliable model performance across different testing scenarios.

In summary, the pre-trained model incorporated more relevant input parameters, compared to the TL model, facilitating the fine-tuning of the initial model to develop the new one. The success of TL from the pullout test to the beam test demonstrates the similarity of the bond mechanism in the two types of tests despite differences in stress states. Thus, the proposed TransTabRegressor framework is well-suited for transferring bond strength prediction from convenient pullout tests to more complex beam tests. Besides, it is important to consider potential biases in the datasets used, as discrepancies between the pullout and beam test datasets, variations in experimental conditions, and measurement errors may influence the model performance.

5.4 | Extensible modelling capacity of TransTabRegressor

The success of TL from 14 parameters of pullout test data to 10 parameters of beam test data was primarily due to the NLP data processor in TransTabRegressor. Conventional ML models require an identical structure of tabular data because they use the number of data columns as the recognition dimension. In these models, parameter names merely serve to distinguish different parameters for researchers.

In contrast, the NLP data processor of TransTabRegressor converts the names of input parameters into tokens, which are then processed into 16-dimensional embeddings. These embeddings are multiplied by the parameter values to create the input data embedding. This method allows the model to capture the semantic information of input parameters, enabling it to recognize parameters based on their semantic context within the dataset. This NLP processing facilitates the recognition of parameters with similar expressions and enables knowledge transfer between models. Thus, the input parameters for TL models transitioning from pullout test data to beam test data can be determined based on specific conditions. This flexibility allows for the building of TL models by adjusting the number of input parameters as needed.

Traditional ML models like XGBoost and NNs are limited in their ability to generalize across datasets with differing input structures. They rely on fixed input dimensions and struggle to interpret the semantic meanings of input parameters, often leading to reduced accuracy when applied to new datasets with variations in parameter names or structures. TransTabRegressor, however, leverages an NLP data processor to embed both parameter names and values, allowing it to recognize and adapt to different expressions of similar parameters. This capability not only reduces the need for extensive feature engineering but also improves the robustness of predictions when transferring learning from one dataset to another. This semantic understanding and adaptability set TransTabRegressor apart from traditional models, enabling more seamless and accurate knowledge transfer.

As shown in Figure 9, the beam test data share some input parameters with the pullout test data. To evaluate

14678667, 2025, 7, Downloaded from https://onlinelibrary.wiley.com/doi/10.1111/mice.13357 by HONG KONG POLYTECHNIC UNIVERSITY HU NG HOM, Wiley Online Library on [11/03/2025]. See the Terms and Conditions (https://onlinelibrary.wiley.com/terms-and-conditions) on Wiley Online Library for rules of use; OA articles are governed by the applicable Creative Commons License

TABLE 12 Evaluation of bond strength TL prediction models using different input parameters.

Input parameter	Model R^2	
	Training set	Testing set
Concrete compressive strength	0.980	0.975
Concrete compressive strengths	0.946	0.944
Concrete strength	0.989	0.902
Compressive strength	0.969	0.913

the ability of the TransTabRegressor framework to capture the semantic information of input parameters, the input parameter "Concrete compressive strength" in the beam test data in case of SF was altered to similar expressions as listed in Table 12. These expressions are similar to the original meaning but are not entirely consistent. TL was then applied to the modified beam test data to predict the bond strength, involving the fine-tuning of the pre-trained model based on pullout test data. The final predicted results of the model are displayed in Table 12. It was observed that the model using the original parameter "Concrete compressive strength" exhibited the best predictive performance. The three models with modified parameter names all achieved R^2 values above 0.9 on the testing set, with "Concrete compressive strengths" having a higher R^2 value than the other two. Semantically, this expression is closest to the original. These results demonstrate that the NLP data processor effectively enhances the recognition of parameters with similar expressions, thereby facilitating knowledge transfer between models.

However, it is important to note that when the parameter was altered to "Concrete strength," there was a noticeable decline in the model's performance as evidenced by a lower R^2 value on the testing set. This drop highlights a current limitation in the semantic recognition capabilities of the TransTabRegressor framework. Although "Concrete strength" and "Concrete compressive strength" are semantically related, the model did not fully recognize them as equivalent. This indicates that in specific scenarios where parameters are contextually similar but not identically phrased, the TransTabRegressor may not perform optimally. This situation underscores the need for enhanced mechanisms within the model to better handle such variations, effectively treating these terms as equivalent.

In summary, the TransTabRegressor framework provides a flexible and scalable solution for extending TL models as more beam test data become available. This framework not only facilitates the transfer of information from simpler pullout tests to more complex and realistic beam tests but also enhances the recognition of input parameters expressed in similar ways. This capability positions TransTabRegressor as a versatile tool for improving the accuracy and robustness of structural predictions across diverse engineering applications.

6 | CONCLUSION

To predict the bond strength of FRP bars in UHPC using limited beam test data, a TransTabRegressor framework was proposed to facilitate transfer learning from pullout to beam test data. The pre-trained model was developed using extensive pullout test data and subsequently fine-tuned with limited beam test data to build the transfer learning model. For comparison, XGBoost and NN models were directly trained on the beam test data. The specific conclusions drawn from the study include:

(1) The bond strength transfer learning models, based on the proposed TransTabRegressor framework, demonstrated great efficiency despite variations in data volume and input parameters. The pre-trained model, built on 479 pullout test data points considering 14 parameters, achieved excellent R^2 values of 0.976 on the training set and 0.951 on the testing set. Fine-tuning this model with 66 data points in case of concrete splitting failure and 49 data points of pullout failure, considering 10 parameters, yielded high R^2 values (training: 0.980, testing: 0.975) for concrete splitting failure and good R^2 values (training: 0.982, testing: 0.955) for pullout failure. These results demonstrate the success of transfer learning from extensive pullout test data to limited beam test data, proving effective knowledge transfer of bond behavior under different stress states.
(2) The transfer learning models demonstrated significant improvements in predictive accuracy, with an 8.5% increase in R^2 on the testing set for concrete splitting failure and a 12.2% increase for pullout failure, compared to models directly trained using XGBoost and NNs. While all models predicted effectively on the training set, the transfer learning models outperformed on the testing set. For concrete splitting failure, the transfer learning model achieved an R^2 value of 0.975, compared to 0.899 for the XGBoost model and 0.887 for the NN model. For pullout failure, the transfer learning model achieved an R^2 value of 0.955, compared to 0.851 for the XGBoost model and 0.849 for the NN model. Additionally, the transfer learning model demonstrated superior performance on the testing set in terms of MAE and RMSE, with lower average predicted errors (4.38% and 5.74% for concrete splitting failure, and 4.07% and 4.69% for pullout failure), compared to XGBoost and NN models, highlighting its robustness and reliability.

14678667, 2025, 7, Downloaded from https://onlinelibrary.wiley.com/doi/10.1111/mice.13357 by HONG KONG POLYTECHNIC UNIVERSITY HU NG HOM, Wiley Online Library on [11/03/2025]. See the Terms and Conditions (https://onlinelibrary.wiley.com/terms-and-conditions) on Wiley Online Library for rules of use; OA articles are governed by the applicable Creative Commons License

(3) With the failure mode prediction model accurately predicting the failure mode of beam test data, a comprehensive process of bond strength prediction can be realized. By precisely predicting the failure mode on beam test data, transfer learning models can be utilized to predict bond strength for concrete splitting or pullout failure mode. It is important to note that dataset biases, such as discrepancies in input parameters and differences in test conditions, may impact the model performance and should be considered in practical applications.

(4) The combination of NLP, transformer, and deep learning in the TransTabRegressor framework revealed flexible and extensive modeling capacity. The selection of input parameters for the transfer learning model can be customized based on the current data conditions. Besides, the framework can effectively capture the semantic information of input parameters, including variations in parameter expressions. This capability enhances the understanding of bond behavior by illustrating how detailed characteristics of FRP bars and UHPC interact, resulting in more accurate and reliable bond strength predictions. However, further improvements are needed in the framework's ability to handle these variations and enhance semantic recognition. This proposed framework provides an effective transfer learning solution for lacking tabular data in engineering applications.

(5) The study highlights the potential of integrating advanced transfer learning and deep learning techniques to address the challenges of limited data and enhance predictive performance. The proposed TransTabRegressor framework effectively utilizes transfer learning, and future research can consider incorporating cutting-edge methods such as neural dynamic classification algorithms, dynamic ensemble learning, and self-supervised learning. These approaches could offer further improvements in handling diverse and complex datasets. The authors are also open to integrating additional deep learning methods as more suitable techniques emerge. Moreover, the framework can be expanded to predict the bond performance from FRP to steel bars in future studies. Continued exploration and adoption of these advanced techniques will be crucial for advancing the field and addressing the evolving challenges in engineering applications.

ACKNOWLEDGMENTS

Thanks to the financial support of the National Natural Science Foundation of China (12072192, U1831105) and the Shanghai Municipal Natural Science Foundation (20ZR1429500).

REFERENCES

ACI Committee 408. (2003). *Bond and development of straight reinforcing bars in tension* (Technical document No. 408R-03). ACI.

ACI Committee 440. (2015). *Guide for the design and construction of concrete reinforced with FRP bars* (Technical document No. 440.1R-15). ACI.

Alam, K. M. R., Siddique, N., & Adeli, H. (2020). A dynamic ensemble learning algorithm for neural networks. *Neural Computing and Applications*, *32*(12), 8675–8690.

Ba, J. L., Kiros, J. R., & Hinton, G. E. (2016). *Layer normalization*. arXiv preprint arXiv:1607.06450. https://doi.org/10.48550/arXiv.1607.06450

Bakouregui, A. S., Mohamed, H. M., Yahia, A., & Benmokrane, B. (2021). Explainable extreme gradient boosting tree-based prediction of load-carrying capacity of FRP-RC columns. *Engineering Structures*, *245*, 112836.

Basaran, B., Kalkan, I., Bergil, E., & Erdal, E. (2021). Estimation of the FRP-concrete bond strength with code formulations and machine learning algorithms. *Composite Structures*, *268*, 113972.

Chen, S. Z., & Feng, D. C. (2022). Multifidelity approach for data-driven prediction models of structural behaviors with limited data. *Computer-Aided Civil and Infrastructure Engineering*, *37*(12), 1566–1581.

Chen, T., & Guestrin, C. (2016). XGBoost: A scalable tree boosting system. *Proceedings of the ACM SIGKDD International Conference on Knowledge Discovery and Data Mining*, San Francisco, CA (pp. 785–794).

Cholakov, R., & Kolev, T. (2022). *The GatedTabTransformer. An enhanced deep learning architecture for tabular modeling*. arXiv preprint arXiv:2201.00199. https://doi.org/10.48550/arXiv.2201.00199

Das, A. K., Suthar, D., & Leung, C. K. Y. (2019). Machine learning based crack mode classification from unlabeled acoustic emission waveform features. *Cement and Concrete Research*, *121*, 42–57.

Devlin, J., Chang, M. W., Lee, K., & Toutanova, K. (2019). BERT: Pre-training of deep bidirectional transformers for language understanding. *NAACL HLT 2019—2019 Conference of the North American Chapter of the Association for Computational Linguistics: Human Language Technologies—Proceedings of the Conference*, Minneapolis, MN (pp. 4171–4186).

Du, J., Meng, W., Khayat, K. H., Bao, Y., Guo, P., Lyu, Z., Abu-obeidah, A., Nassif, H., & Wang, H. (2021). New development of ultra-high-performance concrete (UHPC). *Composites Part B: Engineering*, *224*, 109220.

Gribniak, V., Kaklauskas, G., Torres, L., Daniunas, A., Timinskas, E., & Gudonis, E. (2013). Comparative analysis of deformations and tension-stiffening in concrete beams reinforced with GFRP or steel bars and fibers. *Composites Part B: Engineering*, *50*, 158–170.

Gribniak, V., Mang, H. A., Kupliauskas, R., & Kaklauskas, G. (2015). Stochastic tension-stiffening approach for the solution of serviceability problems in reinforced concrete: Constitutive modeling. *Computer-Aided Civil and Infrastructure Engineering*, *30*(9), 684–702.

Gudonis, E., Kacianauskas, R., Gribniak, V., Weber, A., Jakubovskis, R., & Kaklauskas, G. (2014). Mechanical properties of the bond between GFRP reinforcing bars and concrete. *Mechanics of Composite Materials*, *50*(4), 457–466.

14678667, 2025, 7, Downloaded from https://onlinelibrary.wiley.com/doi/10.1111/mice.13357 by HONG KONG POLYTECHNIC UNIVERSITY HU NG HOM, Wiley Online Library on [11/03/2025]. See the Terms and Conditions (https://onlinelibrary.wiley.com/terms-and-conditions) on Wiley Online Library for rules of use; OA articles are governed by the applicable Creative Commons License

Hernandez Obando, M. D. C., Iqbal, M., Zhang, D., Zhang, P.-F., & Zhao, Q. (2024). Axial strength prediction of seawater sea sand concrete-filled circular FRP tubes under alkaline environment based on ensemble learning algorithms. *Thin-Walled Structures*, *195*, 111530.

Hossain, K. M. A., Ametrano, D., & Lachemi, M. (2017). Bond strength of GFRP bars in ultra-high strength concrete using RILEM beam tests. *Journal of Building Engineering*, *10*, 69–79.

Hossain, K. M. A., Ametrano, D., & Lachemi, M. (2018). The bond between glass-fibre-reinforced polymer bars and ultra-high-strength concrete. *Proceedings of the Institution of Civil Engineers—Construction Materials*, *171*(4), 161–176.

Hu, X., Xue, W., & Xue, W. (2024). Bond properties of GFRP rebars in UHPC under different types of test. *Engineering Structures*, *314*, 118319.

Hu, X., Xue, W., Xue, W., & Jiang, J. (2023). Bond strength of sand-coated deformed GFRP bars in UHPC, HPC, and NC. *Construction and Building Materials*, *403*, 133175.

Huang, B. T., Wang, Y. T., Wu, J. Q., Yu, J., Dai, J. G., & Leung, C. K. Y. (2021). Effect of fiber content on mechanical performance and cracking characteristics of ultra-high-performance seawater sea-sand concrete (UHP-SSC). *Advances in Structural Engineering*, *24*(6), 1182–1195.

Huang, X., Khetan, A., Cvitkovic, M., & Karnin, Z. (2020). *Tab-Transformer: Tabular data modeling using contextual embeddings*. arXiv preprint arXiv:2012.06678. https://doi.org/10.48550/arXiv.2012.06678

Hung, C. C., El-Tawil, S., & Chao, S. H. (2021). A review of developments and challenges for UHPC in structural engineering: Behavior, analysis, and design. *Journal of Structural Engineering (United States)*, *147*(9), 03121001.

Iqbal, M., Zhang, D., Khan, K., Amin, M. N., Ibrahim, M., & Salami, B. A. (2023). Evaluating mechanical, microstructural and durability performance of seawater sea sand concrete modified with silica fume. *Journal of Building Engineering*, *72*, 106583.

Iqbal, M., Zhang, D., Khan, M. I., Zahid, M., & Jalal, F. E. (2023). Effects of rebar size and volume fraction of glass fibers on tensile strength retention of GFRP rebars in alkaline environment via RSM and SHAP analyses. *Journal of Materials in Civil Engineering*, *35*(9), 04023318-1.

Jahangir, H., & Rezazadeh Eidgahee, D. (2021). A new and robust hybrid artificial bee colony algorithm—ANN model for FRP-concrete bond strength evaluation. *Composite Structures*, *257*, 113160.

Jeong, H., Ji, S., Kim, J. H., Choi, S.-H., Heo, I., & Kim, K. S. (2022). Development of mapping function to estimate bond–slip and bond strength of rc beams using genetic programming. *International Journal of Concrete Structures and Materials*, *16*(1), 49.

Jiang, X., & Adeli, H. (2005). Dynamic wavelet neural network for nonlinear identification of highrise buildings. *Computer-Aided Civil and Infrastructure Engineering*, *20*(5), 316–330.

Jung, J., Kim, Y., Park, J., & Ryu, S. (2022). Transfer learning for enhancing the homogenization-theory-based prediction of elasto-plastic response of particle/short fiber-reinforced composites. *Composite Structures*, *285*, 115210.

Kauffman, L., & Fam, A. (2024). Effect of GFRP bar diameter and concrete cover on bond and development length in UHPFRC. *Construction and Building Materials*, *418*, 135445.

Kim, Y. J., & Wang, J. (2022). Interface of ultra-high-performance concrete with steel, glass fiber-reinforced polymer, and basalt fiber-reinforced polymer reinforcing bars. *ACI Structural Journal*, *119*(3), 3–15.

Kingma, D. P., & Ba, J. L. (2015). Adam: A method for stochastic optimization. *3rd International Conference on Learning Representations, ICLR 2015 - Conference Track Proceedings*, San Diego, CA.

Kumar, A., Arora, H. C., & Nehdi, M. L. (2024). XGBoost algorithm based estimation of near surface mounted FRP rod-to-concrete bond strength and failure mode. *Journal of Building Engineering*, *90*, 109418.

Liang, K., Chen, L., Shan, Z., & Su, R. K. L. (2023). Experimental and theoretical study on bond behavior of helically wound FRP bars with different rib geometry embedded in ultra-high-performance concrete. *Engineering Structures*, *281*, 115769.

Lin, B. Y., Lee, S., Khanna, R., & Ren, X. (2020). Birds have four legs?! NumerSense: Probing numerical commonsense knowledge of pre-trained language models. *EMNLP 2020—2020 Conference on Empirical Methods in Natural Language Processing, Proceedings of the Conference*, Online (pp. 6862–6868).

Luo, H., & Paal, S. G. (2021). Reducing the effect of sample bias for small data sets with double-weighted support vector transfer regression. *Computer-Aided Civil and Infrastructure Engineering*, *36*(3), 248–263.

Martins, G. B., Papa, J. P., & Adeli, H. (2020). Deep learning techniques for recommender systems based on collaborative filtering. *Expert Systems*, *37*(6), e12647.

Michaud, D., Fam, A., & Dagenais, M. A. (2021). Development length of sand-coated GFRP bars embedded in ultra-high performance concrete with very small cover. *Construction and Building Materials*, *270*, 121384.

Nan, C., Ruan, H., Ju, X., Hu, J., Liang, L., & Xu, Y. (2024). Transfer-learning-based strategy for enhancing prediction accuracy and computational efficiency of nonlinear mechanical properties in composite materials. *Composites Science and Technology*, *246*, 110388.

Naser, M. Z. (2021). An engineer's guide to eXplainable Artificial Intelligence and Interpretable Machine Learning: Navigating causality, forced goodness, and the false perception of inference. *Automation in Construction*, *129*, 103821.

Naser, M. Z., & Alavi, A. H. (2021). Error metrics and performance fitness indicators for artificial intelligence and machine learning in engineering and sciences. *Architecture, Structures and Construction*, *3*, 499–517.

Nogay, H. S., & Adeli, H. (2021). Detection of epileptic seizure using pretrained deep convolutional neural network and transfer learning. *European Neurology*, *83*(6), 602–614.

Pak, H., Leach, S., Yoon, S. H., & Paal, S. G. (2023). A knowledge transfer enhanced ensemble approach to predict the shear capacity of reinforced concrete deep beams without stirrups. *Computer-Aided Civil and Infrastructure Engineering*, *38*(11), 1520–1535.

Pan, R., Liao, P., Zou, J., Zhou, X., & Li, C. (2022). Experimental investigation on bond performance of helically ribbed GFRP rebar embedded in ultra-high performance concrete. *Construction and Building Materials*, *357*, 129295.

Pan, R., Zou, J., Liao, P., Dong, S., & Deng, J. (2023). Effects of fiber content and concrete cover on the local bond behavior of helically

14678667, 2025, 7, Downloaded from https://onlinelibrary.wiley.com/doi/10.1111/mice.13357 by HONG KONG POLYTECHNIC UNIVERSITY HU NG HOM, Wiley Online Library on [11/03/2025]. See the Terms and Conditions (https://onlinelibrary.wiley.com/terms-and-conditions) on Wiley Online Library for rules of use; OA articles are governed by the applicable Creative Commons License

ribbed GFRP bar and UHPC. *Journal of Building Engineering*, *80*, 107939.

Pan, R. S., Zou, J. Y., Liao, P., & Li, C. X. (2023). Experimental study and calculating method for bond strength between helically ribbed GFRP bar and UHPC. *Zhongguo Gonglu Xuebao/China Journal of Highway and Transport*, *36*(9), 144–156. (in Chinese).

Pan, S. J., & Yang, Q. (2010). A survey on transfer learning. *IEEE Transactions on Knowledge and Data Engineering*, *22*(10), 1345–1359.

Radford, A., Kim, J. W., Hallacy, C., Ramesh, A., Goh, G., Agarwal, S., Sastry, G., Askell, A., Mishkin, P., Clark, J., Krueger, G., & Sutskever, I. (2021). Learning transferable visual models from natural language supervision. *Proceedings of Machine Learning Research*, *139*, 8748–8763.

Raffel, C., Shazeer, N., Roberts, A., Lee, K., Narang, S., Matena, M., Zhou, Y., Li, W., & Liu, P. J. (2020). Exploring the limits of transfer learning with a unified text-to-text transformer. *Journal of Machine Learning Research*, *21*, 1–67.

Rafiei, M. H., & Adeli, H. (2017). A new neural dynamic classification algorithm. *IEEE Transactions on Neural Networks and Learning Systems*, *28*(12), 3074–30837990591.

Rafiei, M. H., & Adeli, H. (2018). A novel unsupervised deep learning model for global and local health condition assessment of structures. *Engineering Structures*, *156*, 598–607.

Rafiei, M. H., Gauthier, L. V., Adeli, H., & Takabi, D. (2024). Self-supervised learning for electroencephalography. *IEEE Transactions on Neural Networks and Learning Systems*, *35*(2), 1457–1471.

Rafiei, M. H., Khushefati, W. H., Demirboga, R., & Adeli, H. (2016). Neural network, machine learning, and evolutionary approaches for concrete material characterization. *ACI Materials Journal*, *113*(6), 781–789.

Rafiei, M. H., Khushefati, W. H., Demirboga, R., & Adeli, H. (2017). Novel approach for concrete mixture design using neural dynamics model and virtual lab concept. *ACI Materials Journal*, *114*(1), 117–127.

RILEM TC. (1994). RC5 bond test for reinforcement steel. 1. Beam test. In *RILEM Technical Recommendations for the testing and use of construction materials*. E & FN Spon, 213–217.

Rossini, M., Saqan, E., & Nanni, A. (2019). Prediction of the creep rupture strength of GFRP bars. *Construction and Building Materials*, *227*, 116620.

Saleh, S., Mahmood, A. H., Hamed, E., & Zhao, X. L. (2023). The mechanical, transport and chloride binding characteristics of ultra-high-performance concrete utilising seawater, sea sand and SCMs. *Construction and Building Materials*, *372*, 130815.

Sayed-Ahmed, M., & Sennah, K. (2016). Bond strength of ribbed-surface high-modulus glass FRP bars embedded into unconfined UHPFRC. *Proceedings, Annual Conference—Canadian Society for Civil Engineering*, *3*, 2317–2326.

Sayed Ahmed, M., & Sennah, K. (2015). Pullout strength of sand-coated GFRP bars embedded in ultra-high performance fiber reinforced concrete. *Proceedings, Annual Conference—Canadian Society for Civil Engineering*, *3*, 1604–1613.

Shafighfard, T., Kazemi, F., Bagherzadeh, F., Mieloszyk, M., & Yoo, D. Y. (2024). Chained machine learning model for predicting load capacity and ductility of steel fiber–reinforced concrete beams. *Computer-Aided Civil and Infrastructure Engineering*, *39*, 23.

Shin, H. C., Roth, H. R., Gao, M., Lu, L., Xu, Z., Nogues, I., Yao, J., Mollura, D., & Summers, R. M. (2016). Deep convolutional neural networks for computer-aided detection: CNN architectures, dataset characteristics and transfer learning. *IEEE Transactions on Medical Imaging*, *35*(5), 1285–1298.

Teng, J. G., Xiang, Y., Yu, T., & Fang, Z. (2019). Development and mechanical behaviour of ultra-high-performance seawater sea-sand concrete. *Advances in Structural Engineering*, *22*(14), 3100–3120.

Thai, H. T. (2022). Machine learning for structural engineering: A state-of-the-art review. *Structures*, *38*, 448–491.

Tong, D., Chi, Y., Huang, L., Zeng, Y., Yu, M., & Xu, L. (2023). Bond performance and physically explicable mathematical model of helically wound GFRP bar embedded in UHPC. *Journal of Building Engineering*, *69*, 106322.

Vaswani, A., Shazeer, N., Parmar, N., Uszkoreit, J., Jones, L., Gomez, A. N., Kaiser, Ł., & Polosukhin, I. (2017). Attention is all you need. *Advances in Neural Information Processing Systems, 2017*, Long Beach, CA (pp. 5999–6009).

Wambeke, B. W., & Shield, C. K. (2006). Development length of glass fiber-reinforced polymer bars in concrete. *ACI Structural Journal*, *103*(1), 11–17.

Wang, Z., & Sun, J. (2022). TransTab: Learning transferable tabular transformers across tables. *Advances in Neural Information Processing Systems*, *35*, New Orleans, LA.

Xu, Y., Weng, H., Ju, X., Ruan, H., Chen, J., Nan, C., Guo, J., & Liang, L. (2021). A method for predicting mechanical properties of composite microstructure with reduced dataset based on transfer learning. *Composite Structures*, *275*, 114444.

Yan, F., Lin, Z. B., Wang, X. Y., Azarmi, F., & Sobolev, K. (2017). Evaluation and prediction of bond strength of GFRP-bar reinforced concrete using artificial neural network optimized with genetic algorithm. *Composite Structures*, *161*, 441–452.

Yoo, D. Y., Kwon, K. Y., Park, J. J., & Yoon, Y. S. (2015). Local bond-slip response of GFRP rebar in ultra-high-performance fiber-reinforced concrete. *Composite Structures*, *120*, 53–64.

Yoo, D. Y., & Yoon, Y. S. (2017). Bond behavior of GFRP and steel bars in ultra-high-performance fiber-reinforced concrete. *Advanced Composite Materials*, *26*(6), 493–510.

Yoo, S. J., Hong, S. H., Yoo, D. Y., & Yoon, Y. S. (2024). Flexural bond behavior and development length of ribbed CFRP bars in UHPFRC. *Cement and Concrete Composites*, *146*, 105403.

Yoo, S. J., Hong, S. H., & Yoon, Y. S. (2023). Bonding behavior and prediction of helically ribbed CFRP bar embedded in ultra high-performance concrete (UHPC). *Case Studies in Construction Materials*, *19*, e02253.

Zeng, J. J., Feng, P., Dai, J. G., & Zhuge, Y. (2022a). Development and behavior of novel FRP-UHPC tubular members. *Engineering Structures*, *266*, 114540.

Zeng, J. J., Liao, J., Zhuge, Y., Guo, Y. C., Zhou, J. K., Huang, Z. H., & Zhang, L. (2022b). Bond behavior between GFRP bars and seawater sea-sand fiber-reinforced ultra-high strength concrete. *Engineering Structures*, *254*, 113787.

Zhang, F., Wang, C., Liu, J., Zou, X., Sneed, L. H., Bao, Y., & Wang, L. (2023). Prediction of FRP-concrete interfacial bond strength based on machine learning. *Engineering Structures*, *274*, 115156.

Zhang, P.-F., Iqbal, M., Zhang, D., Zhao, X.-L., & Zhao, Q. (2024). Bond strength prediction of FRP bars to seawater sea sand concrete based on ensemble learning models. *Engineering Structures*, *302*, 117382.

14678667, 2025, 7, Downloaded from https://onlinelibrary.wiley.com/doi/10.1111/mice.13357 by HONG KONG POLYTECHNIC UNIVERSITY HU NG HOM, Wiley Online Library on [11/03/2025]. See the Terms and Conditions (https://onlinelibrary.wiley.com/terms-and-conditions) on Wiley Online Library for rules of use; OA articles are governed by the applicable Creative Commons License

Zhang, P.-F., Zhao, X.-L., Zhang, D., Iqbal, M., Zhao, X., Zhao, Q., Tuerxunmaimaiti, Y., & Yu, C. (2024). Prediction of bond strength and failure mode of FRP bars embedded in UHPC or UHPSSC utilising extreme gradient boosting technique. *Composite Structures*, *346*, 118437.

Zhang, Z., Liu, Q., & Wu, D. (2022). Predicting stress–strain curves using transfer learning: Knowledge transfer across polymer composites. *Materials and Design*, *218*, 110700.

Zhao, Q., Zhang, D. X., Zhao, X. L., & Sharma, S. (2021). Modelling damage evolution of carbon fiber-reinforced epoxy polymer composites in seawater sea sand concrete environment. *Composites Science and Technology*, *215*, 108961.

Zhao, Q., Zhao, X.-L., Zhang, D., Dai, J.-G., & Xue, X. (2024). Degradation of GFRP bars with epoxy and vinyl ester matrices in a marine concrete environment: An experimental study and theoretical modeling. *Journal of Composites for Construction*, *28*(2), 04024004.

Zhao, Q., Zhao, X.-L., Zhang, D., & Duan, L. (2024). Effects of exposure in seawater sea-sand concrete pore solution on fatigue performance of carbon FRP bars. *Composites Science and Technology*, *247*, 110418.

Zou, X., & Chung, E. (2024). Traffic prediction via clustering and deep transfer learning with limited data. *Computer-Aided Civil and Infrastructure Engineering*, *39*(17), 2683–2700.

How to cite this article: Zhang, P.-F., Zhang, D., Zhao, X.-L., Zhao, X., Iqbal, M., Tuerxunmaimaiti, Y., & Zhao, Q. (2025). Natural language processing-based deep transfer learning model across diverse tabular datasets for bond strength prediction of composite bars in concrete. *Computer-Aided Civil and Infrastructure Engineering*, *40*, 917–939. https://doi.org/10.1111/mice.13357

14678667, 2025, 7, Downloaded from https://onlinelibrary.wiley.com/doi/10.1111/mice.13357 by HONG KONG POLYTECHNIC UNIVERSITY HU NG HOM, Wiley Online Library on [11/03/2025]. See the Terms and Conditions (https://onlinelibrary.wiley.com/terms-and-conditions) on Wiley Online Library for rules of use; OA articles are governed by the applicable Creative Commons License